

**IMPROVING THE IMPINGEMENT COLD PLATE  
THERMAL DESIGN USING  
NUMERICAL AND ANALYTICAL APPROACH**

by

REUBEN JOSHUA MADHUKER

THESIS

Submitted in partial fulfilment of the requirements  
for the degree of Master of Science in Mechanical Engineering at  
The University of Texas at Arlington  
May 2021

Arlington, Texas

Supervising Committee:

Dr. Dereje Agonafer, Supervising Professor

Dr. Abdolhossein Haji-Sheikh

Dr. Rajesh Kasukurthy

Copyright © by  
Reuben Joshua Madhuker  
2021



# **ABSTRACT**

## **IMPROVING THE IMPINGEMENT COLD PLATE THERMAL DESIGN USING NUMERICAL AND ANALYTICAL APPROACH**

Reuben Joshua Madhuker, MS

The University of Texas at Arlington, 2021

Supervising Professor: Dr. Dereje Agonafer

Conventional cooling methods for an IC chip uses heat spreader to transfer heat from the chip end of the spreader to the opposite end of the spreader which then uses air or water to remove heat and thereby maintaining the overall temperature. Unfortunately, the heat spreader itself has constraints such as conduction resistance which adds the heat spreader inefficiency. But if we increase the area exposed to the cooling end then this can be improved. This is done by introducing channels at that end. These channels act as fins which give a better shot at cooling the system temperature. These channels are classified according to their geometry.

This study basically presents improving the impingement cold plate thermal design using analytical and numerical approach. For this, a cold plate resting on a heat dissipating chip has been taken and on top of the cold plate, two heat sinks are placed on it leaving a certain distance in between them for the incoming water flow. During experimentation, the heat from the IC chip passes through the cold plate and transfers to the heat sinks which is cooled by water. A detailed analysis of the influence of change in inlet conditions and heat

sink geometry on inlet velocity, pressure drop and maximum temperature has been carried out. pressure drop, temperature rise and thermal resistance across the cold plates have been measured by running simulation on ANSYS Icepak which have been then compared to the numerical results obtained. A number of simulations have been run to obtain the optimum size of mesh grids in ANSYS Icepak to be able to use for the different models to get the best result.

## **ACKNOWLEDGEMENT**

All glory to the Almighty Lord. It has been well said that if a person desires to do something and achieves his goal, it is his duty to acknowledge the people who helped him in his journey.

I sincerely thank my Supervising Professor, Dr. Dereje Agonafer, who gave me this awesome opportunity to learn and shape my academic career under him. I thank him for giving me invaluable tips that will definitely help me ahead in my future. I also thank him for always providing me with opportunities to connect with experts and learn through them whether in lectures or research work.

I especially thank Dr. Abdolhossein Haji-Sheikh and Dr. Rajesh Kasukurthy for serving as my committee members and showing me how I can better myself in my work.

I thank the whole brilliant EMNSPC team of Dr. Dereje Agonafer who helped in my research work. A special thanks to Dr. Uschas Chowdhury who helped me a lot throughout my Thesis and being there for me.

I thank the Mechanical and Aerospace Engineering at The University of Texas at Arlington for giving be excellent opportunities to study and learn a lot under different Professors who have always motivated me to do something better.

May 05, 2021

## **DEDICATION**

All glory to the Almighty Lord for giving me the wisdom to understand and learn and the strength to complete my work. I dedicate this work to my mother, Jagruti Madhuker and father, Joshua Madhuker. I thank them for believing in me and being constant role models for me. A word of thanks for my friends for always supporting me and cheering me up.

# TABLE OF CONTENTS

<b>TITLE</b>	<b>PAGE NO.</b>
<b>ABSTRACT</b> .....	<b>I</b>
<b>ACKNOWLEDGEMENT</b> .....	<b>III</b>
<b>DEDICATION</b> .....	<b>IV</b>
<b>TABLE OF CONTENTS</b> .....	<b>V</b>
<b>LIST OF FIGURES</b> .....	<b>VII</b>
<b>LIST OF TABLES</b> .....	<b>IX</b>
<b>NOMENCLATURE</b> .....	<b>X</b>
<b>CHAPTER 1: INTRODUCTION</b> .....	<b>1</b>
<b>CHAPTER 2: PROBLEM SETUP</b> .....	<b>5</b>
<b>2.1 Classification of microchannels</b> .....	<b>5</b>
<b>2.2 Defining geometry</b> .....	<b>6</b>
<b>2.3 Assumptions</b> .....	<b>10</b>
<b>CHAPTER 3: ANALYTICAL APPROACH</b> .....	<b>11</b>
<b>CHAPTER 4: NUMERICAL APPROACH</b> .....	<b>16</b>
<b>4.1 Initial problem setup</b> .....	<b>18</b>
<b>4.2 Initial solution:</b> .....	<b>18</b>
<b>4.3 Mesh Sensitivity Analysis</b> .....	<b>22</b>
<b>4.4 Change in geometry and flow parameters</b> .....	<b>28</b>
<b>4.4.1 Change in inlet width</b> .....	<b>28</b>

4.4.2 Change in flow rate.....	30
4.4.3 Change in fin thickness .....	33
<b>CHAPTER 5: POST-PROCESSING OF RESULTS.....</b>	<b>37</b>
<b>CHAPTER 6: CONCLUSION.....</b>	<b>38</b>
<b>REFERENCES.....</b>	<b>39</b>



# LIST OF FIGURES

<b>FIGURES</b>	<b>PAGE NO.</b>
Figure 1 Heat Spreader and Heat Sink on Flip Chip Package .....	1
Figure 2 ANSYS Icepak model of the setup .....	6
Figure 3 Close view of thin adiabatic plates .....	6
Figure 4 Enclosure encapsulating the microchannel array along with inlet and outlet openings .....	7
Figure 5 Heat source .....	7
Figure 6 Close view of microchannel array with base and height dimensions.....	9
Figure 7 Close view of microchannel array with fin dimensions.....	9
Figure 8 Close view of microchannels.....	11
Figure 9 Theoretical representation of microchannel for analysis .....	11
Figure 10 Fanning friction factor and Nusselt number for fully developed laminar flow .....	13
Figure 11 Contraction and expansion loss coefficients for flow between inlet and outlet manifolds .....	15
Figure 12 ANSYS Icepak Model.....	16
Figure 13 Separate mesh assembly near the fins .....	17
Figure 14 Variation of Temperature in Y plane .....	19
Figure 15 Variation of Temperature in Z plane .....	20
Figure 16 Variation of Pressure in Y plane .....	20
Figure 17 Location of maximum and minimum temperature .....	21
Figure 18 Location of maximum and minimum pressure.....	21
Figure 19 Slack variable setting for separate mesh assembly.....	22
Figure 20 Variation in Maximum Temperature w.r.t. change in number of nodes .....	23

<b>Figure 21 Variation in Maximum Pressure w.r.t. change in number of nodes.....</b>	<b>23</b>
<b>Figure 22 Variation in Thermal Resistance of fins w.r.t. change in number of nodes.....</b>	<b>24</b>
<b>Figure 23 Pressure Variation in particular microchannels observed in XZ-plane .....</b>	<b>26</b>
<b>Figure 24 Direction of mass flow in XZ-plane.....</b>	<b>26</b>
<b>Figure 25 Direction of mass flow in XZ-plane near outlet .....</b>	<b>27</b>
<b>Figure 26 Magnitude of Pressure in XZ-plane near inlet and outlet .....</b>	<b>27</b>
<b>Figure 27 Variation in Maximum Temperature w.r.t. change in inlet width .....</b>	<b>28</b>
<b>Figure 28 Variation in Maximum Pressure w.r.t. change in inlet width .....</b>	<b>29</b>
<b>Figure 29 Variation in Thermal Resistance of fins w.r.t. change in inlet width .....</b>	<b>29</b>
<b>Figure 30 Variation in Maximum Temperature of other components w.r.t. change in inlet width.....</b>	<b>30</b>
<b>Figure 31 Variation in Maximum Temperature w.r.t. change in flow rate .....</b>	<b>31</b>
<b>Figure 32 Variation in Maximum Pressure w.r.t. change in inlet width .....</b>	<b>32</b>
<b>Figure 33 Variation in Thermal Resistance of fins w.r.t. change in flow rate .....</b>	<b>32</b>
<b>Figure 34 Variation in Maximum Temperature of other components w.r.t. change in flow rate .....</b>	<b>33</b>
<b>Figure 35 Variation in Maximum Temperature w.r.t. change in fin thickness .....</b>	<b>34</b>
<b>Figure 36 Variation in Maximum Pressure w.r.t. change in fin thickness .....</b>	<b>35</b>
<b>Figure 37 Variation in Thermal Resistance of fins w.r.t. change in fin thickness .....</b>	<b>35</b>
<b>Figure 38 Variation in Maximum Temperature of other components w.r.t. change in fin thickness.....</b>	<b>36</b>

# LIST OF TABLES

<b>TABLES</b>	<b>PAGE NO.</b>
<b>Table 1 Classification of channels .....</b>	<b>5</b>
<b>Table 2 Geometrical Dimensions of the parts .....</b>	<b>8</b>
<b>Table 3 Values of different parameters from initial solution .....</b>	<b>19</b>
<b>Table 4 Comparison of Parameter values before and after mesh sensitivity analysis ....</b>	<b>25</b>
<b>Table 5 Reynolds number and Peclet number for different flow rates .....</b>	<b>31</b>
<b>Table 6 Fin thickness and number of fins per array .....</b>	<b>34</b>

## NOMENCLATURE

P	pressure (Pa)
H	channel height (m)
$f_{app}$	apparent friction coefficient
$f$	friction coefficient
L	heat sink length (m)
$D_h$	hydraulic diameter (m)
p	Wetted perimeter
h	heat transfer coefficient (W/m <sup>2</sup> .K)
$W_{pp}$	pumping power (W)
v	velocity at inlet (m/s)
$u_m$	Mean flow velocity in channel (m/s)
A	area (m <sup>2</sup> )
$\Delta P$	pressure drop (Pa)
Q	Flow rate (m <sup>3</sup> /s)
k	thermal conductivity (W/m.K)
$R_{tot}$	total thermal resistance (K/W)
Re	Reynolds number
Pe	Peclet number
Po	Hagen–Poiseuille number
T	temperature (K)
W	heat sink width (m)
$C_p$	specific heat capacity (J/kg.K)
$W_c$	channel width (m)
n	number of channels
$q_{max}$	maximum heat flux (W/m <sup>2</sup> )
$L_h$	Hydrodynamic developing region
$X_{hyd}$	dimensionless axial distance for hydrodynamic entrance region
Nu	Nusselt number
$W_w$	channel wall thickness (m)
$t_b$	base thickness (m)
$\mu$	dynamic viscosity (kg/m.s)
$\rho$	density (kg/m <sup>3</sup> )
$\eta_f$	fin efficiency
$\alpha_c$	channel aspect ratio

# CHAPTER 1

## INTRODUCTION

One of the most important aspects of electronics packaging is the thermal management of electronic devices. The advancement in microelectronics technology has been rapid and due to this the volume occupied by the devices has reduced considerably. Further, with the increasing demand for faster and more efficient processors, the number of circuits and the power dissipation per unit volume has also increased. As a result of this, the heat flux from the chip surface to be removed has increased. So, here the high heat dissipating devices need to be maintained at a desired junction temperature limit to achieve higher thermal reliability and sustained functionality. There is also a desire to reduce the junction temperature as the increased temperature adversely affects the electrical performance of the devices and reduces their reliability the possible damage involves junction fatigue changes in electrical parameters and thermal runaway. [5-6,8]

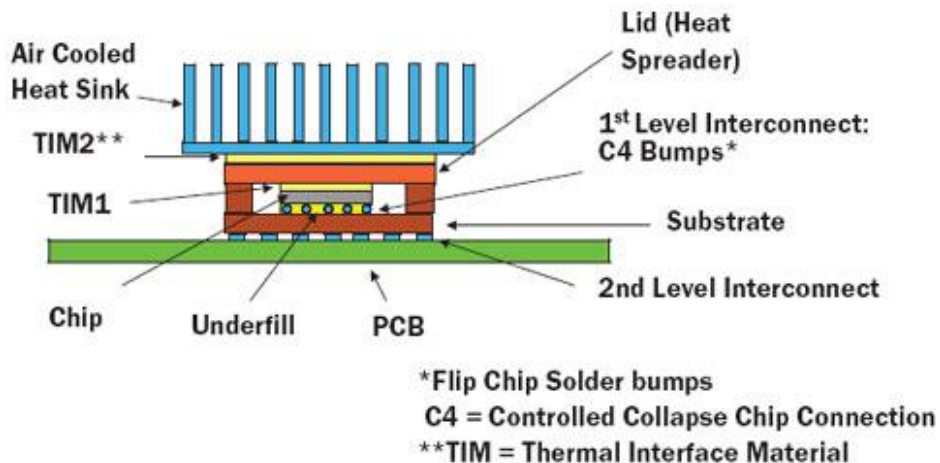


Figure 1 Heat Spreader and Heat Sink on Flip Chip Package

Now instead of a single processor chip consider a data centre. Many cooling systems have been employed such as Calibrated Vecteded Cooling (CVC), Chilled water system, Cold

aisle/Hot aisle containment, Computer Room Air Conditioner (CRAC), Computer Room Air Handler (CRAH), Evaporative cooling, Raised floor, Liquid cooling technologies such as Immersion cooling and Direct-to-chip cooling. Air has been the first choice of fluid in such cooling applications but direct cooling of chips offers a practical solution to the heat dissipation problem. The reason for going to liquid cooling is that the IT equipment simply cannot be cooled to its temperature requirements any longer with air because modern data centres mostly have high power density equipment and therefore increased cooling is required. So, in such systems, water is circulated in microchannels fabricated on the chip substrate microchannel heat sinks for cooling such high heat dissipating devices are particularly attractive as they are compact lightweight and offer large surface to volume ratio higher surface to volume ratio results in enhanced cooling performance. So, these systems need to be carefully designed to meet the cooling requirements under the operational constraints.

When liquid cooling is considered, it depends on many different parameters such as targets of performance, power delivery, energy efficiency requirements, IT equipment density, compute density, cooling costs, future IT equipment needs and strategy. An important design consideration is to ensure that the cooling liquid which is used should never be mixed with any other cooling liquid, since the integrity of the cooling liquid is of uttermost importance to ensure the longevity of the cooling liquid. Water with additives and glycol-based liquids are mostly used as coolants for single-phase cooling while dielectric liquids and certain refrigerants can be used for both single-phase and two-phase cooling. The selection of cooling liquid is based on operational need, material compatibility with the wetted materials in all cooling components, IT equipment serviceability, cooling liquid maintenance need, life expectancy and liquid cost. [7]

Water with additives is used because of the good heat transfer properties of water and the additives are chemicals added to reduce corrosion risk and bacterial growth. These

additives can reduce the heat transfer properties of the water, and potential impact to overall performance should be investigated. Another property of water is its freezing point at 0°C. It is therefore important to know the operating range of the liquid and temperature requirement/exposure during shipping and storage.[7]

Glycol based liquids are liquids where glycol is added to lower the freezing temperature and reduce bacterial growth. Commonly used glycols are ethylene glycol and propylene glycol. Propylene glycol is preferred since it is less toxic than ethylene glycol. In small quantities, the propylene glycol is even used in the food industry as an additive.[7]

Dielectric liquids can be used for both single-phase and two-phase cooling. Liquids with higher boiling temperatures operate in single-phase, while liquids with lower boiling temperatures operate in two-phase. The boiling/saturation temperature of the liquids can be altered by varying the operating pressure. One advantage with dielectric liquids is that in the event of a potential leak, the liquid is an electric insulator and does not short the electronic circuits of the IT equipment. Often these liquids have higher density, cost more and have higher Global Warming Potential (GWP). These affects should be considered in the analysis when selecting coolant liquid. [7]

In addition to dielectric liquids, refrigerants can also be used for two-phase cooling. The refrigerants have relatively low boiling temperature that allows the liquid to change phase and evaporate. Again, this saturation temperature can be altered by varying the operating pressure.[7]

In this work, a comprehensive and systematic robust analytical methodology for design and optimization of microchannel heat sinks has been discussed. The analytical method helps to predict transport phenomena such as Nusselt number, heat transfer coefficient, total thermal resistance and pressure drops of the microchannel heat sinks with arbitrarily located semiconductor devices. Also, both fully developed and simultaneously

developing flow through the microchannel heat sink are considered to delineate their relative effect on the pertinent transport phenomena. The flow is considered to be single-phase and laminar for the range of the flow Reynolds number ( $Re$ ).

Apart from the analytical approach, the numerical approach has also been studied which involves running simulations on ANSYS Icepak. A variety of parameters related to the cold plate optimization such as fin thickness and spacing, flow rate and inlet width have been varied and results have been obtained. The effects of varying these parameters have been studied for maximum pressure, temperature and thermal resistance.



# CHAPTER 2

## PROBLEM SETUP

### 2.1 Classification of microchannels:

In this work, the channels on the chip substrate that are considered for analysis are microchannels. There is a certain classification of these channels which make them stand apart from each other. The classification is given below.

**Table 1 Classification of channels [6]**

<b>CHANNEL TYPE</b>	<b>SIZE (Based on Hydraulic Diameter D)</b>
Conventional channels	$D > 3\text{mm}$
Minichannels	$3\text{mm} \geq D \geq 300\mu\text{m}$
<b>Microchannels</b>	<b><math>300\mu\text{m} \geq D \geq 10\mu\text{m}</math></b>
Transitional microchannels	$10\mu\text{m} \geq D \geq 1\mu\text{m}$
Transitional nanochannels	$1\mu\text{m} \geq D \geq 0.1\mu\text{m}$
Nanochannels	$\geq 0.1\mu\text{m} \geq D$

The hydraulic diameter is the defining parameter of the microchannel and according to the setup, microchannel is the correct definition for the channels used here.

## 2.2 Defining geometry:

The following figures show the various important parts of the geometry. They are modelled in ANSYS Icepak.

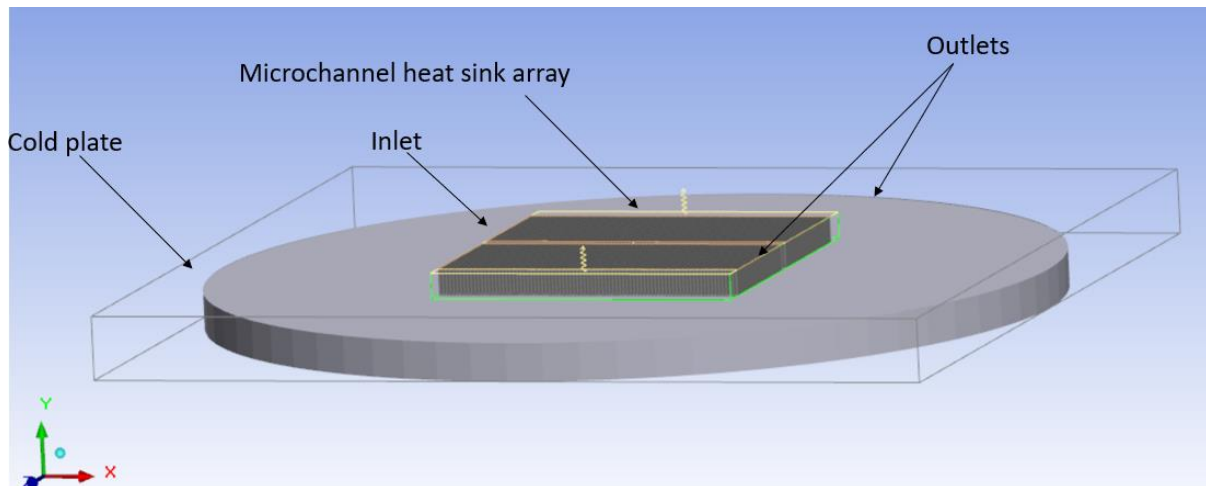


Figure 2 ANSYS Icepak model of the setup

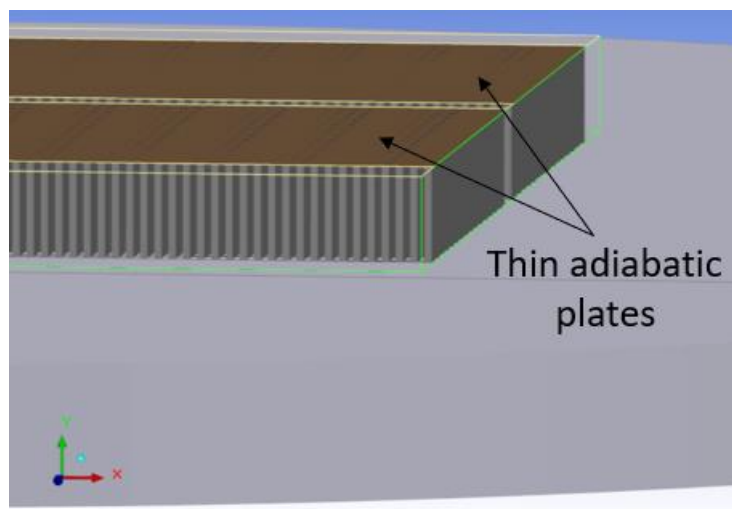
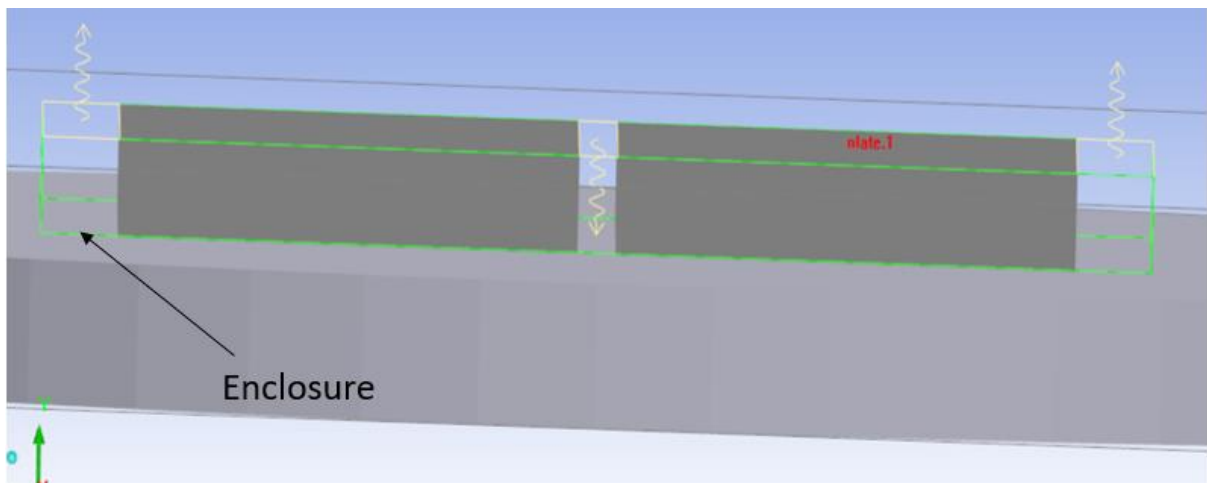
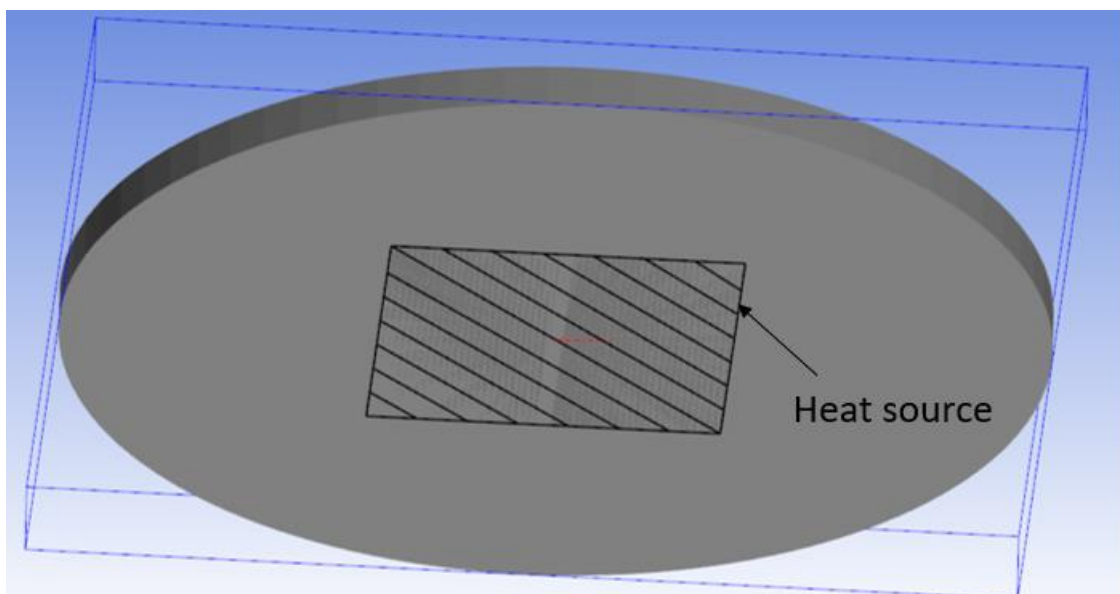


Figure 3 Close view of thin adiabatic plates



**Figure 4** Enclosure encapsulating the microchannel array along with inlet and outlet openings

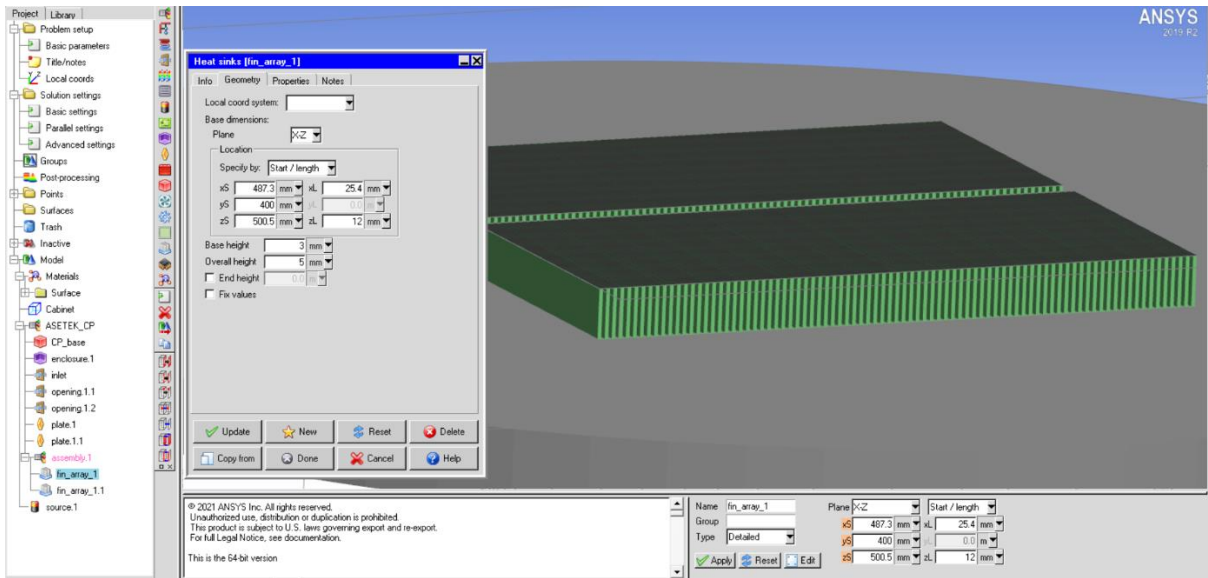


**Figure 5** Heat source

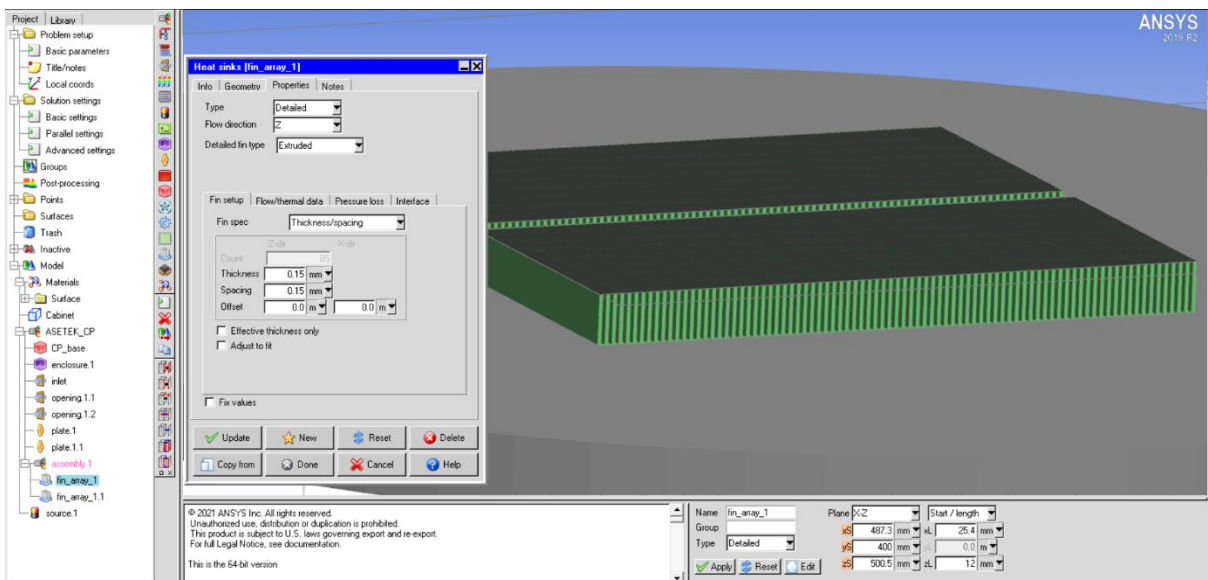
The following table states the geometrical dimensions of the important parts. It is important to notice that the setup is considerably small. This is because its application is also done where more cooling is required within a small area i.e. power density is high in that area.

**Table 2 Geometrical Dimensions of the parts**

<b>Geometry Parts</b>	<b>Dimensions</b>
Cabinet	$0.07*0.005*0.07 \text{ m}^3$
Cold plate base (Cu)	0.035m Radius, 0.003m thick
Enclosure	$0.0254*0.002*0.029 \text{ m}^3$
Inlet area	$0.0254*0.001 \text{ m}^2$
Outlet area 1,2	$0.0254*0.002 \text{ m}^2$
Thin adiabatic plates 1,2	$0.0254*0.012 \text{ m}^2$
Heat Source	$0.0254*0.0254 \text{ m}^2$



**Figure 6 Close view of microchannel array with base and height dimensions**



**Figure 7 Close view of microchannel array with fin dimensions**

Fig. 6 and 7 show the close view of microchannel array with their dimensions. As one can see in fig. 6, the microchannel is just 2mm in height and the cold plate base is 3mm in height. The overall configuration height is just 5mm. Fig. 7 shows the thickness and spacing between the fins. The initial setup has 0.15mm thick fins and 0.15mm as fin gap.

According to the hydraulic diameter formula which is  $D_h = 4A/p$ , the area of the microchannel here is  $0.15 \times 2 \text{ mm}^2$  and wetted perimeter is 4.3mm. So, the  $D_h$  value is  $279 \mu\text{m}$  which is well appropriate in the range of definition of microchannels.

Further, from fig. 7, it can be seen that the initial number of fins is 85 per array. So, in total, 170 fins have been taken in consideration for analysis initially.

### **2.3 Assumptions:**

While setting up the problem, the following assumptions have been taken into consideration.

- 1) Constant heat flux on the channel walls – The boundary condition on the microchannel walls is assumed to be axially constant wall heat flux with circumferentially constant wall temperature. The heat flux along the length of the channel is constant, while the wall temperature varies along the channel length in the flow direction.
- 2) Heat losses from the thin adiabatic plates are neglected – The thin adiabatic plates on the microchannels are assumed to be insulated and hence the fin tip can be considered to be under adiabatic tip boundary condition.
- 3) The coolant flow is steady and incompressible – The working fluid is water at 280K and the maximum pressure drop is generally less than 100 kPa, so, the incompressible flow assumption should be valid.
- 4) Uniform heat flux over the active chip surface area is assumed with no local hotspots.
- 5) A single-phase flow of water with split-flow arrangement of microchannels is considered.
- 6) A constant heat source of 500W has been taken.

# CHAPTER 3

## ANALYTICAL APPROACH

In this approach, basically, the pressure drop in the microchannel that will be used can be calculated using a certain set of equations while keeping the inlet conditions constant. Here, let's start with a flow of 1 litre/min at inlet of the geometry which is basically  $Q$ .

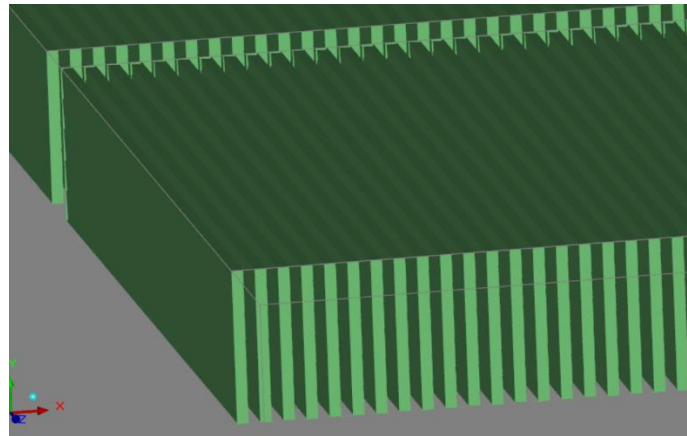


Figure 8 Close view of microchannels

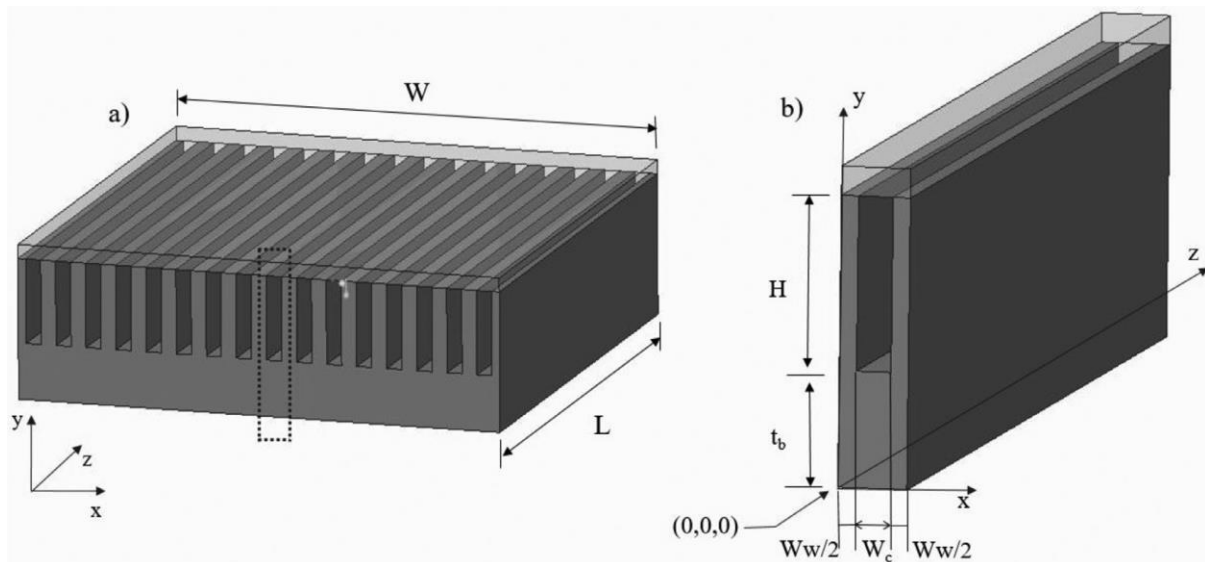


Figure 9 Theoretical representation of microchannel for analysis [5]

This flow splits in two as it is a split flow arrangement after passing through inlet section. The inlet area is known from the geometry so, the inlet velocity can be found by

using  $Q=A*v$ . It comes around 0.656 m/s in negative Y-direction (considering the geometry axes). As, this flow splits, so the velocity be according to the new split flow and inlet area of the microchannels which is basically the aspect ratio.

For proceeding further in analysis, we need to know the type of flow. This can be determined by calculating the Reynolds number (Re). Re is found by the equation,

$Re = (\rho*v*D_h)/\mu$ . Here, all the parameters are known so the calculating Re will give us an idea of type of flow. In this case, the flow will be laminar.

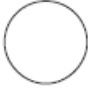
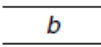
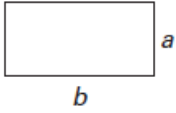

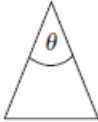
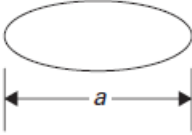
In practice, the flow enters as developing laminar flow and after a certain length, it becomes fully developed laminar flow. This length,  $L_h$  is the hydrodynamic developing region and it can be calculated by using the formula  $(L_h/ D_h) = 0.05*Re$ . This value comes around 6.4 mm for initial case for a total channel length of 12 mm.

The velocity gradient at the channel wall can be readily calculated from the well-known Hagen–Poiseuille parabolic velocity profile for the fully developed laminar flow. The result for friction factor  $f$  is presented in the form for rectangular ducts:

$$Po = fRe = 24(1 - 1.3553 \alpha_c + 1.9467 \alpha_c^2 - 1.7012 \alpha_c^3 + 0.9564 \alpha_c^4 - 0.2537 \alpha_c^5) \quad (3.1)$$

This depends on the flow channel geometry. The Fanning friction factor and Nusselt number for fully developed laminar flow in ducts with cross-section of different shapes is shown in fig. 10.



Duct shape		$Nu_H$	$Nu_T$	$Po = fRe$	
	Circular	4.36	3.66	16	
	Flat channel	8.24	7.54	24	
	Rectangular, aspect ratio, $b/a =$	1	3.61	2.98	14.23
		2	4.13	3.39	15.55
		3	4.79	3.96	17.09
		4	5.33	4.44	18.23
		6	6.05	5.14	19.70
		8	6.49	5.60	20.58
	Hexagon	4.00	3.34	15.05	
	Isosceles Triangle, Apex angle $\theta =$	10°	2.45	1.61	12.47
		30°	2.91	2.26	13.07
		60°	3.11	2.47	13.33
		90°	2.98	2.34	13.15
		120°	2.68	2.00	12.74
	Ellipse, Major/Minor axis $a/b =$	1	4.36	3.66	16.00
		2	4.56	3.74	16.82
		4	4.88	3.79	18.24
		8	5.09	3.72	19.15
		16	5.18	3.65	19.54

$Nu = hD_h/k$ ;  $Re = \rho u_m D_h/\mu$ ;  $Nu_H$  –  $Nu$  under a constant heat flux boundary condition, constant axial heat flux, and uniform circumferential temperature;  $Nu_T$  –  $Nu$  under a constant wall temperature boundary condition;  $f$  – friction factor.

**Figure 10 Fanning friction factor and Nusselt number for fully developed laminar flow in ducts with cross-section of different shapes [9]**

So, for the fully developed laminar flow the pressure drop  $\Delta P$  is given by the equation

$$\Delta p = \frac{2f\rho u_m^2 L}{D} \quad (3.2)$$

But an apparent friction factor,  $f_{app}$ , accounts for the pressure drop due to friction and the developing region effects. It represents an average value of the friction factor over the flow length between the entrance section and the location under consideration. Thus, the

pressure drop in a channel of hydraulic diameter  $D_h$  over a length  $x$  from the entrance is expressed as:

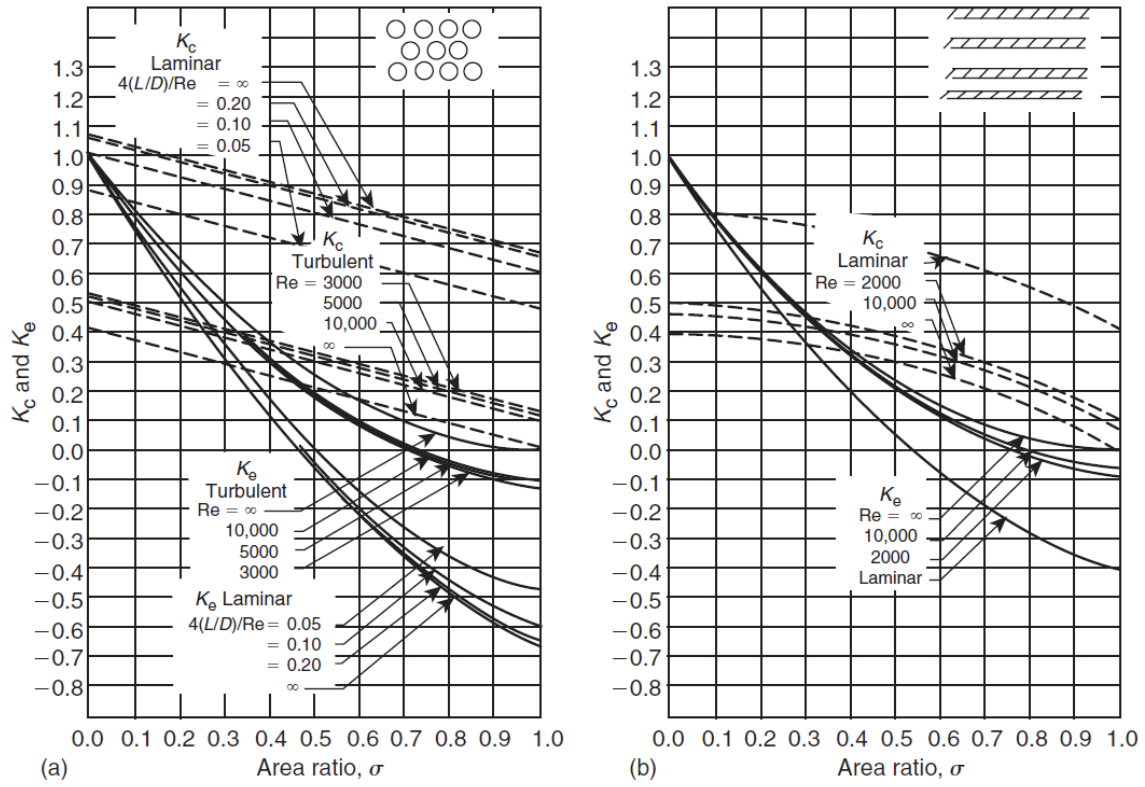
$$\Delta p = \frac{2f_{app}\rho u_m^2 x}{D_h} \quad (3.3)$$

Further, this is for an individual straight path in the microchannel. But the resulting pressure drop measurement should represent the combined effect of the losses in the bends, entrance and exit losses, developing region effects, and the core frictional losses. Thus, the measured pressure drop is the sum of these components and is given by

$$\Delta p = \frac{\rho u_m^2}{2} \left[ (A_c/A_p)^2 (2K_{90}) + (K_c + K_e) + \frac{4f_{app}L}{D_h} \right] \quad (3.4)$$

Here,  $A_c$  is the channel area,  $A_p$  is the plenum area and  $K_{90}$ ,  $K_c$  and  $K_e$  are the loss coefficients at  $90^\circ$  bends, contraction area and expansion area. Also,  $f_{app}$  includes the combined effects of frictional losses and the additional losses in the developing flow region. The following chart in fig. 10 can be used to find out these coefficients.

The total pressure drop  $\Delta P$  in this way comes around 930 Pa. At the inlet part, the pressure drop is 368 Pa while at the fins, it is 562 Pa.



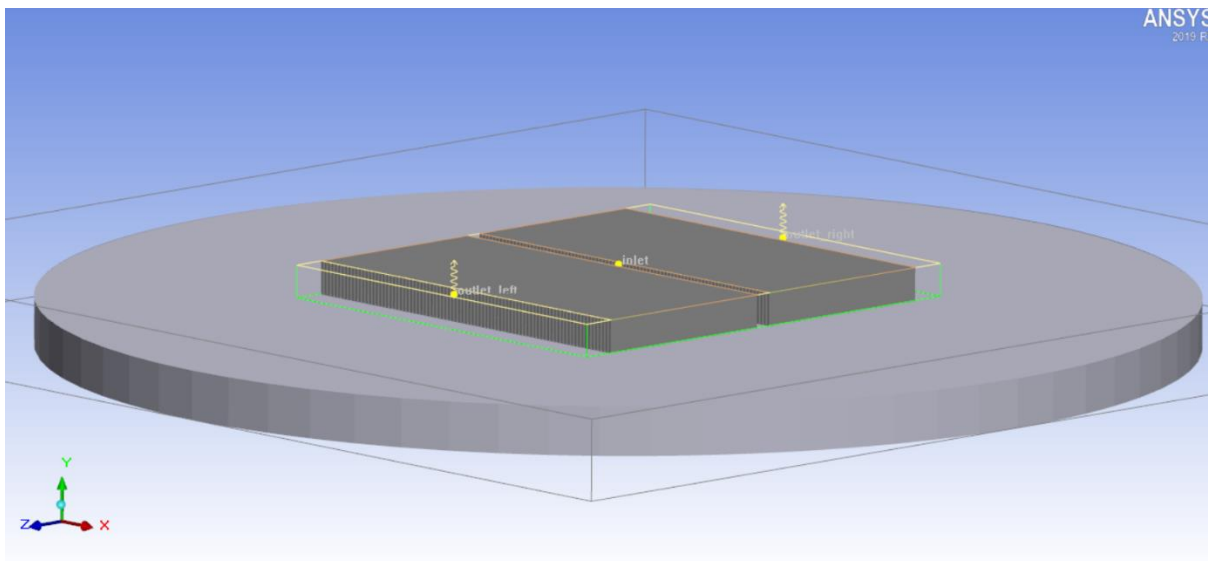
**Figure 11 Contraction and expansion loss coefficients for flow between inlet and outlet manifolds and the microchannels [9]**

Further, if we want to optimise the pressure drop value, we take the help of the values of  $Nu$  and  $Po$  given in fig. 10. For certain aspect ratios, we have values of  $Nu$  and  $Po$  given. Using that we can design for specific microchannels to lower the pressure drop value which better a flow and increases the overall efficiency of the microchannel.

# CHAPTER 4

## NUMERICAL APPROACH

Basically, this approach concentrates in running a number of simulations for a variety of changes in the cold plate parameters and getting the optimum result out of it. The volume within the enclosure encompassing the inlet and outlet openings as well as the microchannels is analysed. Monitor points are set to observe incoming and outgoing flow rates. Each part of the setup has its own maximum and minimum temperature that can be observed in solution report. Thermal resistance for each part of the geometry can be observed. Plane cuts in different planes passing through the geometry help observe how the temperature and pressure varies. All these observations will be under steady state conditions.



**Figure 12 ANSYS Icepak Model**

As the volume within the enclosure encompassing the inlet and outlet openings as well as the microchannels is analysed, separate mesh assembly for the fin array is used which is shown in fig. 13.

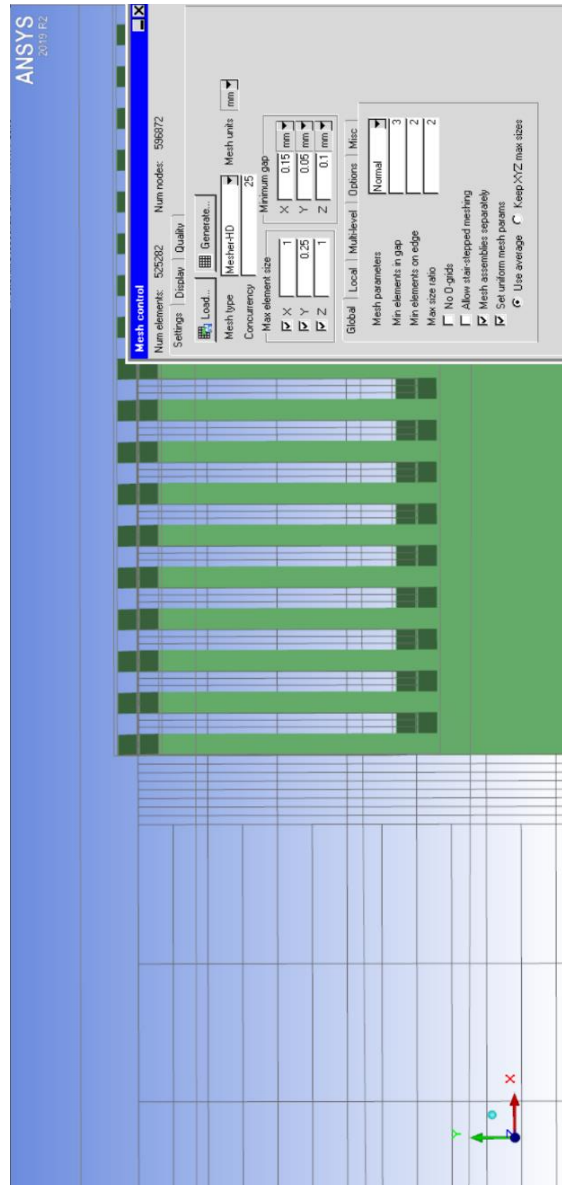


Figure 13 Separate mesh assembly near the fins

#### **4.1 Initial problem setup:**

Similar to analytical approach, initial flow rate has been set as 1 litre/min. Default fluid as water at 280K is taken. Downward gravity vector as per geometry has been set. Further, ambient temperature of 25 °C has been considered. Since, inlet and outlet areas have been defined, it is forced convection. heat transfer due to radiation has been ignored for solution. Steady state condition is used.

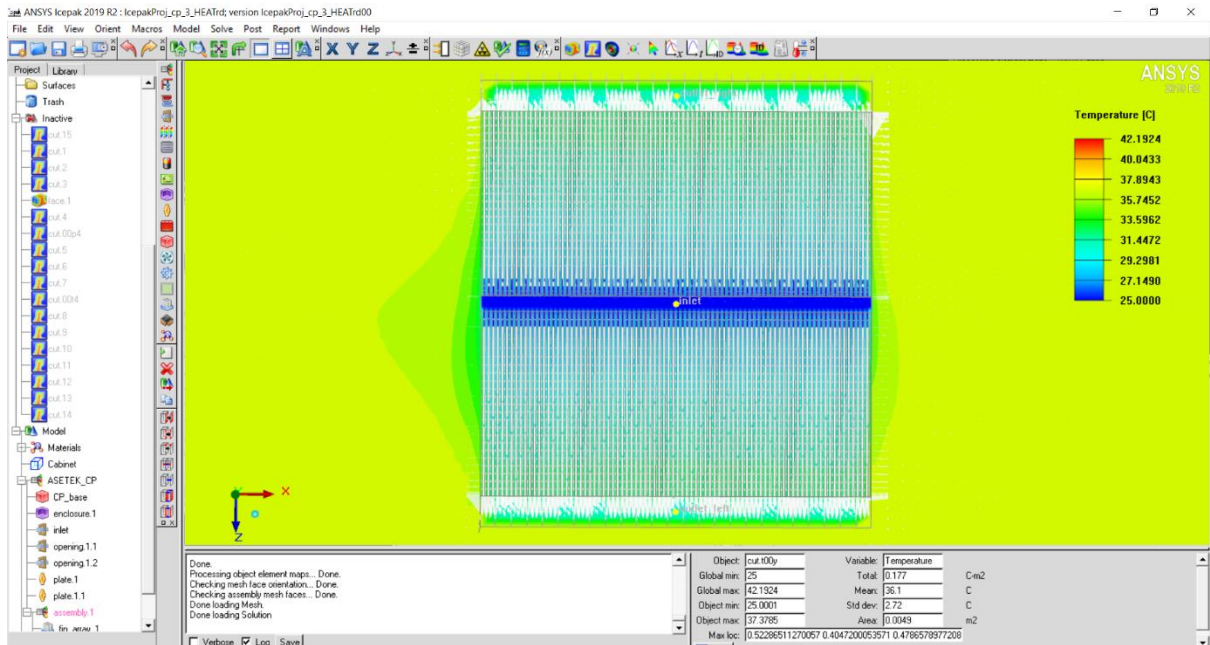
Further, the Reynolds number and Peclet number for this initial run are 461 and 4731 respectively which are obtained from Icepak.

#### **4.2 Initial solution:**

The maximum temperature values for different parts of the geometry, the thermal resistance of the fins and the maximum pressure that were obtained while running the initial simulation are shown in table 3. The variation of temperature and pressure in different planes and location of maximum and minimum temperature and pressure have been shown in the figures after table 3.

**Table 3 Values of different parameters from initial solution**

Parameter	Value
Cold plate base temperature	39.85955 °C
Enclosure temperature	37.36001 °C
Fin array 1 temperature	42.14315 °C
Fin array 1.1 temperature	42.19244 °C
(Thin adiabatic) Plate 1 temperature	37.28387 °C
(Thin adiabatic) Plate 1.1 temperature	37.02963 °C
Heat source temperature	42.19244 °C
Thermal resistance of fin array 1	0.0714521 °C/W
Thermal resistance of fin array 1.1	0.0716158 °C/W
Maximum pressure	3139.11 Pa



**Figure 14 Variation of Temperature in Y plane**

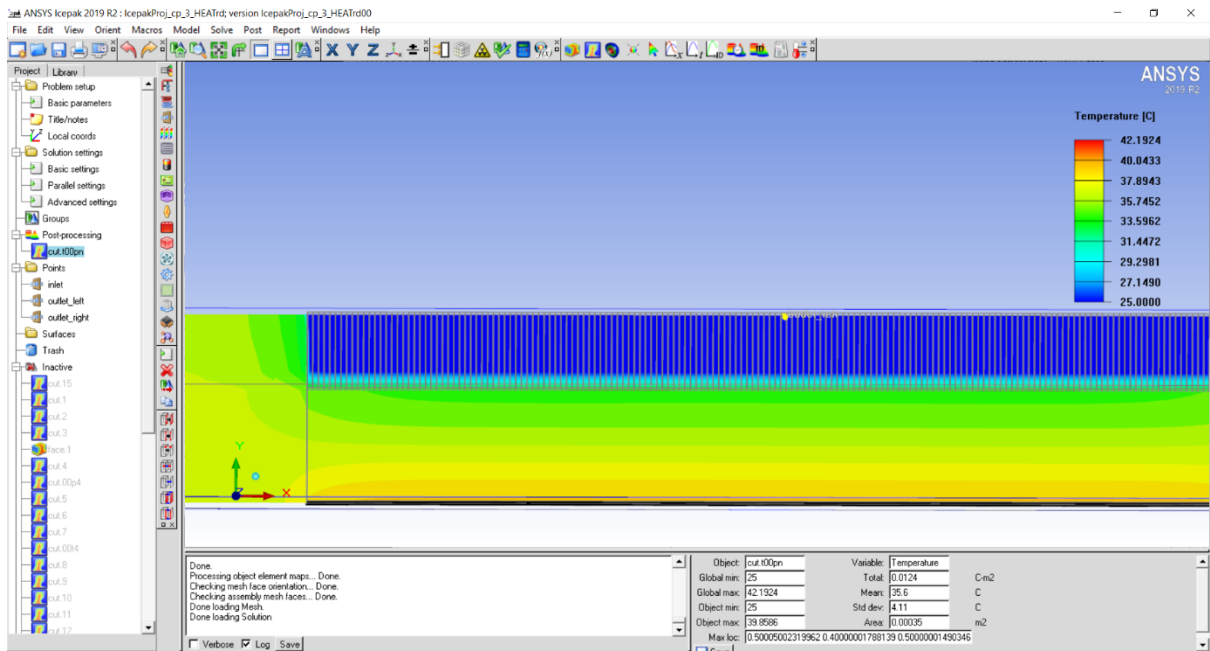


Figure 15 Variation of Temperature in Z plane

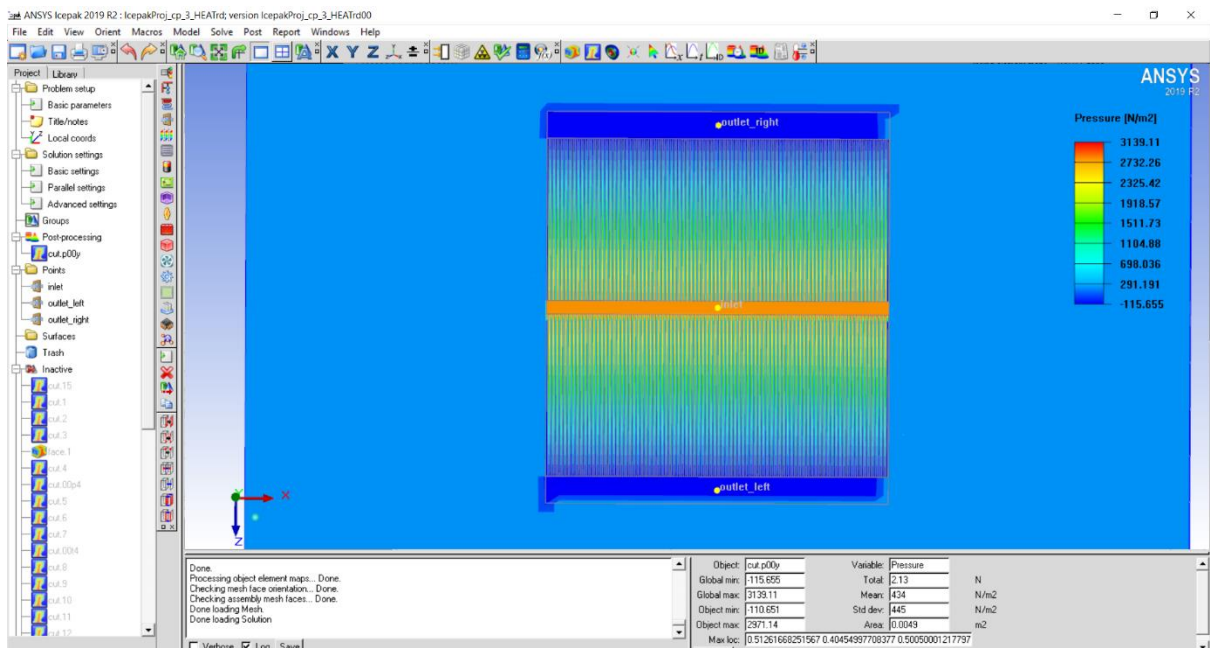


Figure 16 Variation of Pressure in Y plane



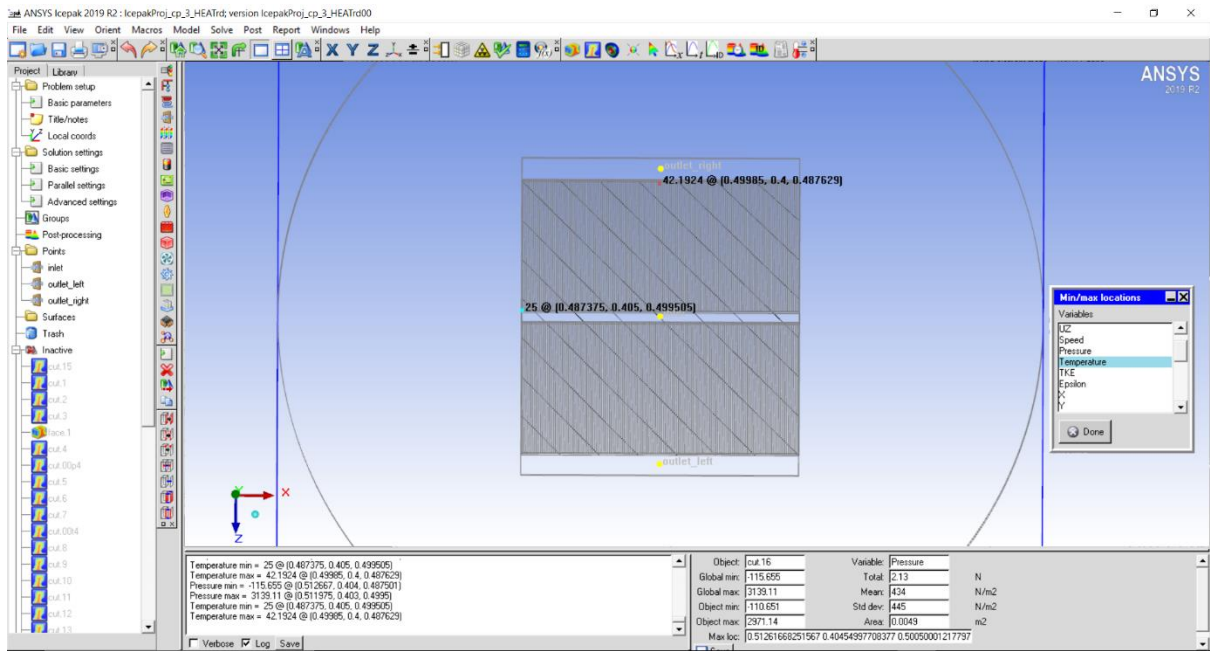


Figure 17 Location of maximum and minimum temperature

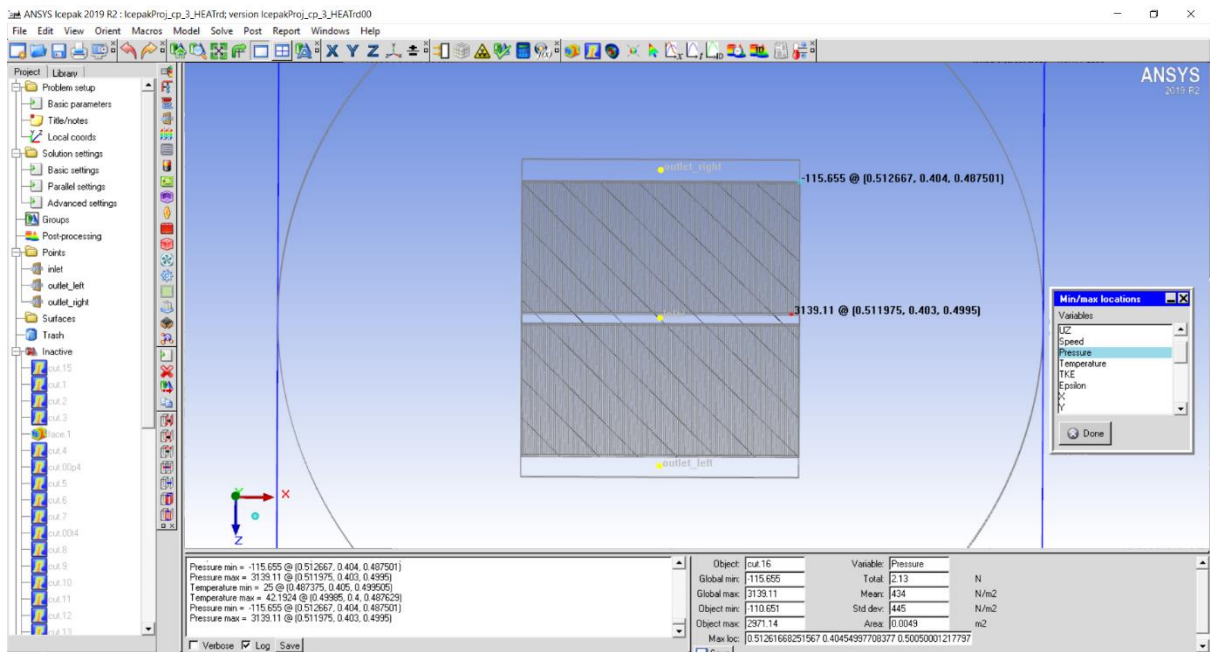
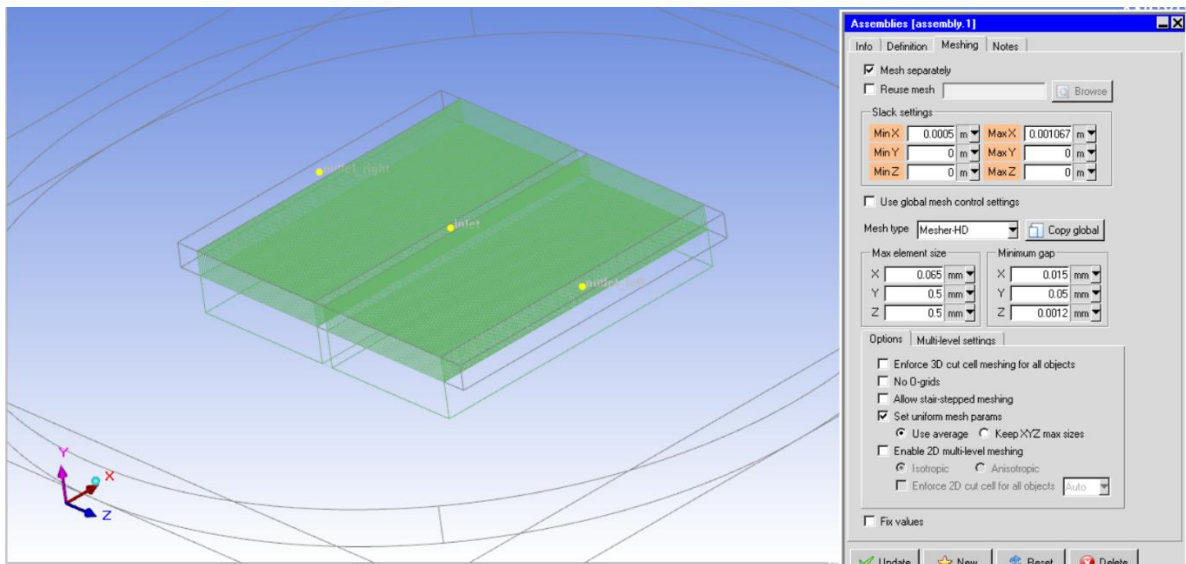


Figure 18 Location of maximum and minimum pressure

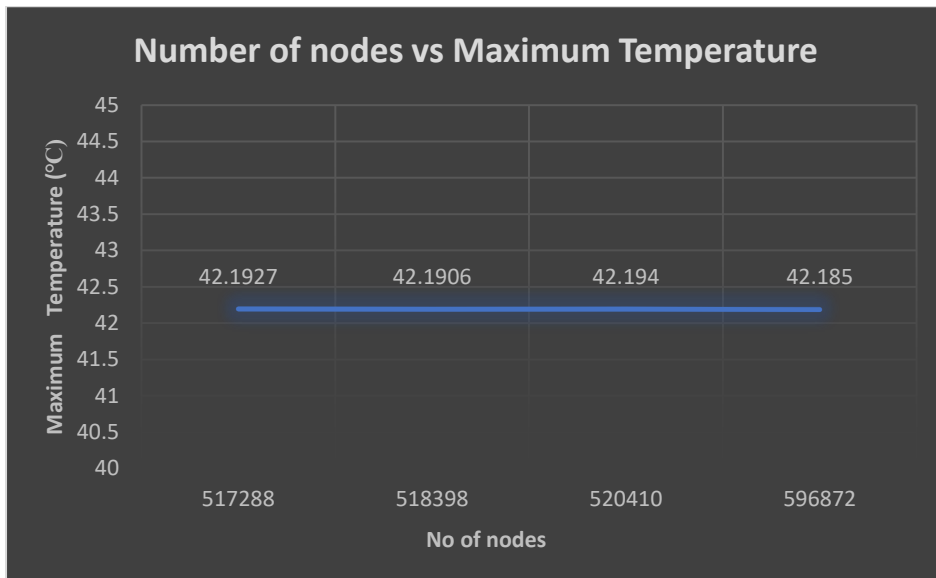
### 4.3 Mesh Sensitivity Analysis:

Icepak provides us a further option in the separate mesh assembly to change the slack variable settings. This means that the separate mesh grid assembly can have varied mesh grid size in all X, Y and Z directions. So, for this part, a mesh sensitivity analysis has been done for a particular problem setup by modifying the mesh to smaller and smaller sizes and results have been observed. The slack variable setting is shown in fig. 19. In our case, uniform mesh parameter setting is considered. Also, multilevel meshing with maximum 3 layers is set with zero buffer layers.

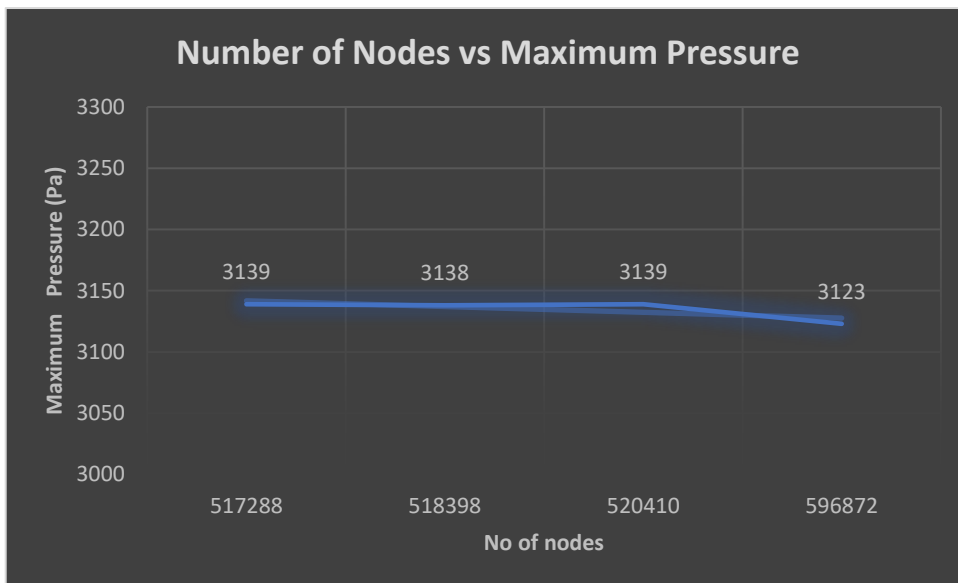


**Figure 19 Slack variable setting for separate mesh assembly**

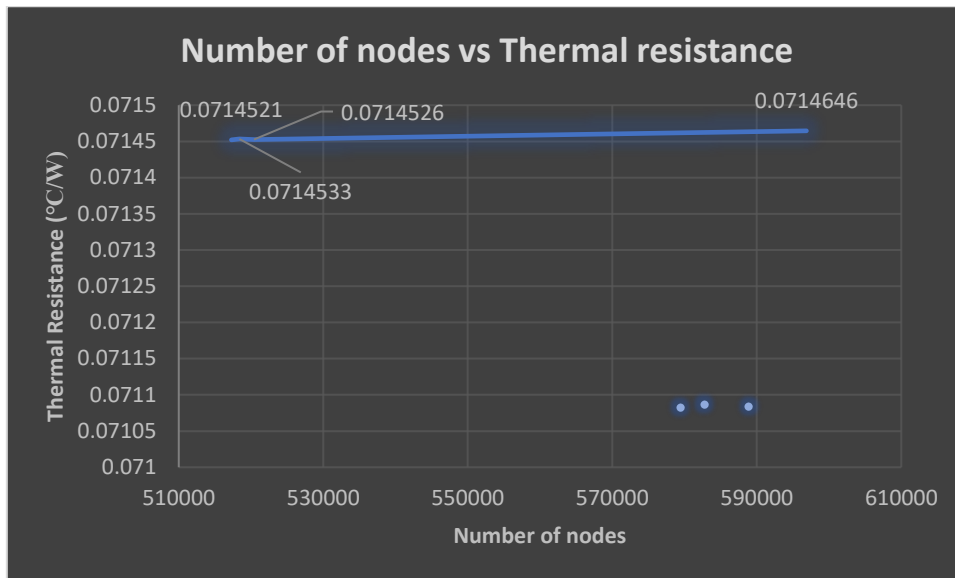
The following figures show the improvement in the value of maximum temperature, maximum pressure and thermal resistance of fins after mesh sensitivity analysis. Here, the same problem setup is simulated but with finer mesh grids each time for the separate mesh assembly shown in fig. 19.



**Figure 20** Variation in Maximum Temperature w.r.t. change in number of nodes



**Figure 21** Variation in Maximum Pressure w.r.t. change in number of nodes



**Figure 22** Variation in Thermal Resistance of fins w.r.t. change in number of nodes

A comparison of parameter values before and after doing mesh sensitivity analysis is shown in table 4. It has been noticed that although the values are not same but they are nearly same.

**Table 4 Comparison of Parameter values before and after mesh sensitivity analysis**

<b>Parameter</b>	<b>Value before</b>	<b>Values after</b>	<b>% difference</b>
Cold plate base temperature	39.85955 °C	39.8601 °C	0.00165
Enclosure temperature	37.36001 °C	37.35034 °C	0.000259
Fin array 1 temperature	42.14315 °C	42.14614 °C	0.0067
Fin array 1.1 temperature	42.19244 °C	42.18649 °C	0.014
(Thin adiabatic) Plate 1 temperature	37.28387 °C	37.22714 °C	0.1523
(Thin adiabatic) Plate 1.1 temperature	37.02963 °C	36.89785 °C	0.3571
Heat source temperature	42.19244 °C	42.1865 °C	0.0141
Thermal resistance of fin array 1	0.0714521 °C/W	0.0714646 °C/W	0.0175
Thermal resistance of fin array 1.1	0.0716158 °C/W	0.071591 °C/W	0.0346
Maximum pressure	3139.11 Pa	3123 Pa	0.5123

The pressure variation and mass flow direction within the microchannels after doing mesh sensitivity analysis have been shown in the figures below.

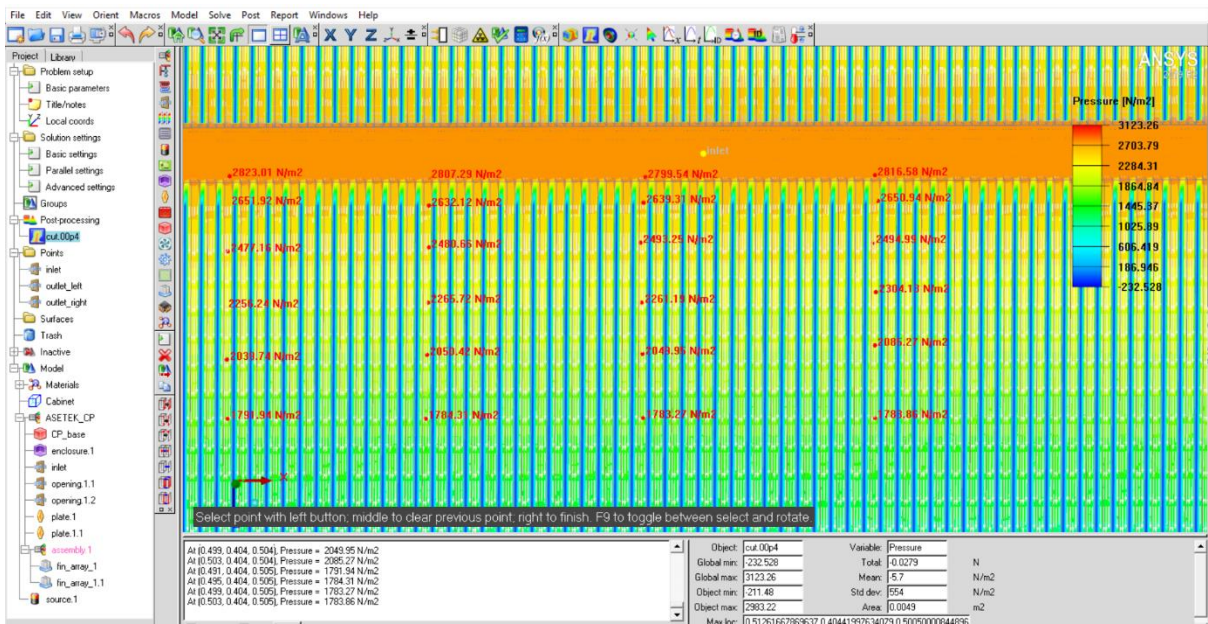


Figure 23 Pressure Variation in particular microchannels observed in XZ-plane

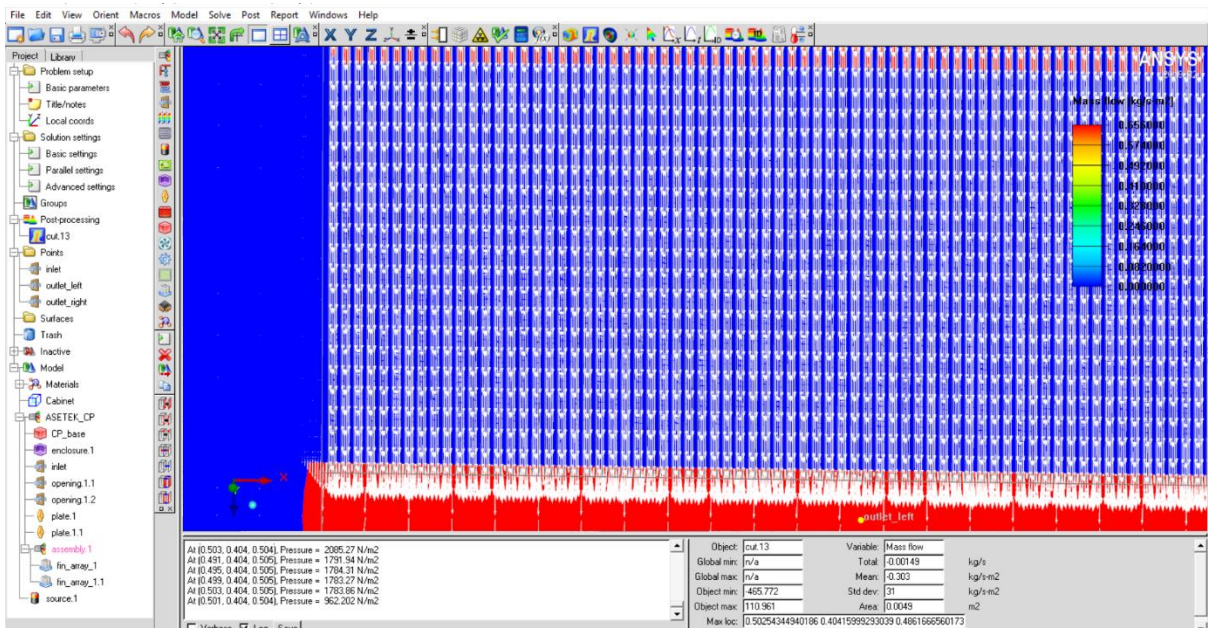


Figure 24 Direction of mass flow in XZ-plane

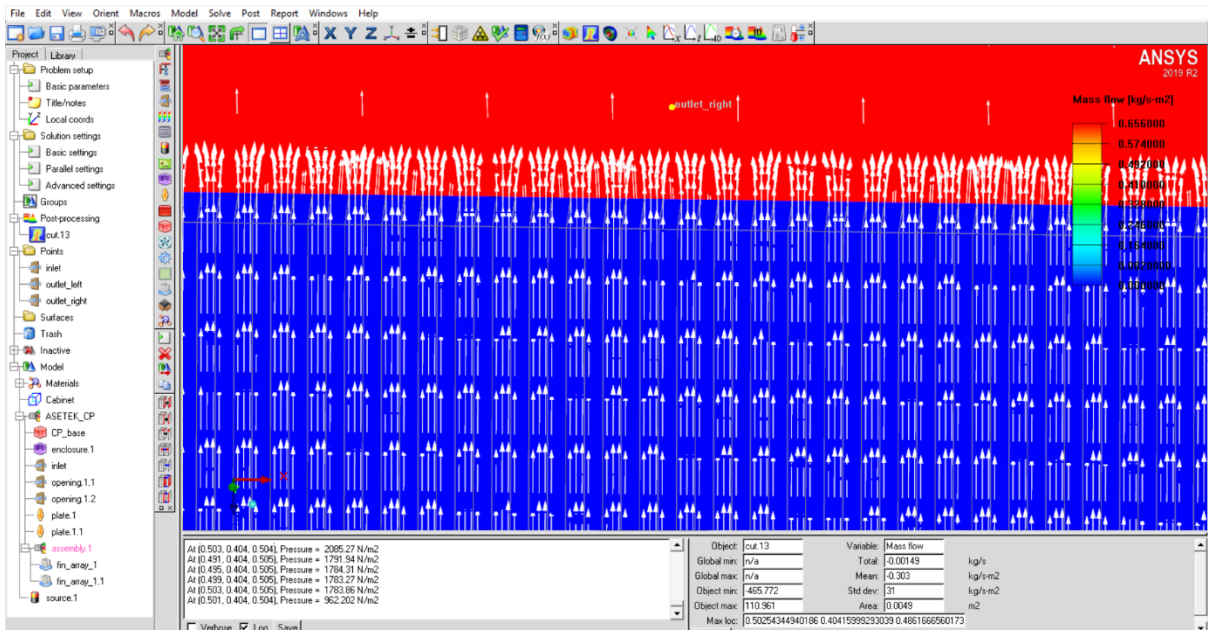


Figure 25 Direction of mass flow in XZ-plane near outlet

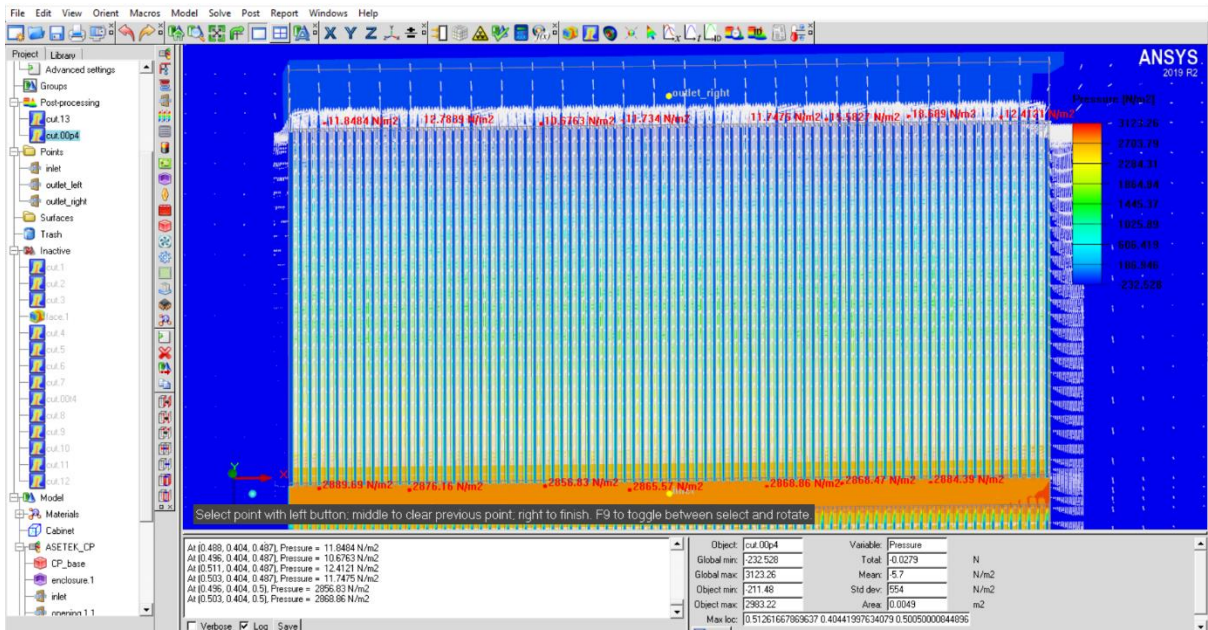


Figure 26 Magnitude of Pressure in XZ-plane near inlet and outlet

## 4.4 Change in geometry and flow parameters:

Moving further ahead in optimization, to observe the effects of change in geometry and flow parameters, it is necessary that the model that was analysed for mesh sensitivity be used. This means that finer mesh with small slack variables be used for getting the best results.

### 4.4.1 Change in inlet width:

Here, the effect of varying the inlet width on maximum temperature, pressure and thermal resistance is observed keeping the flow rate same as the original one. Hence, there is no change in Reynolds number and Peclet number. The following figures show how different inlet width have impact on these parameters.

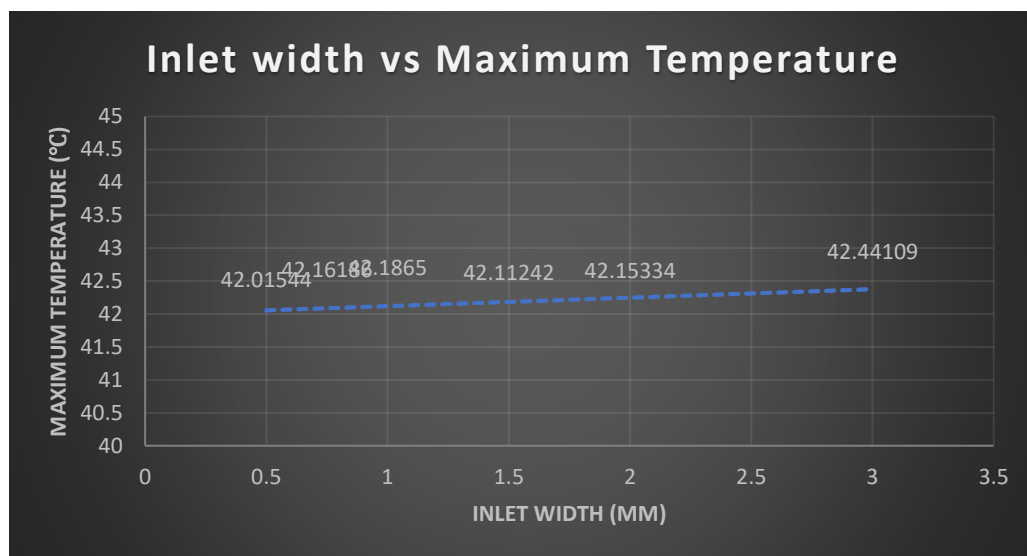
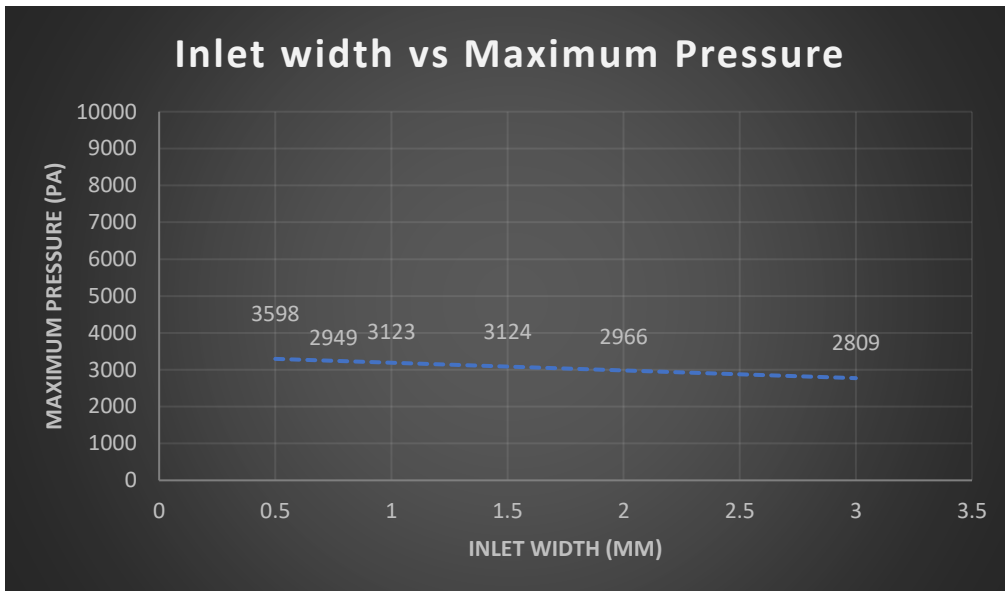
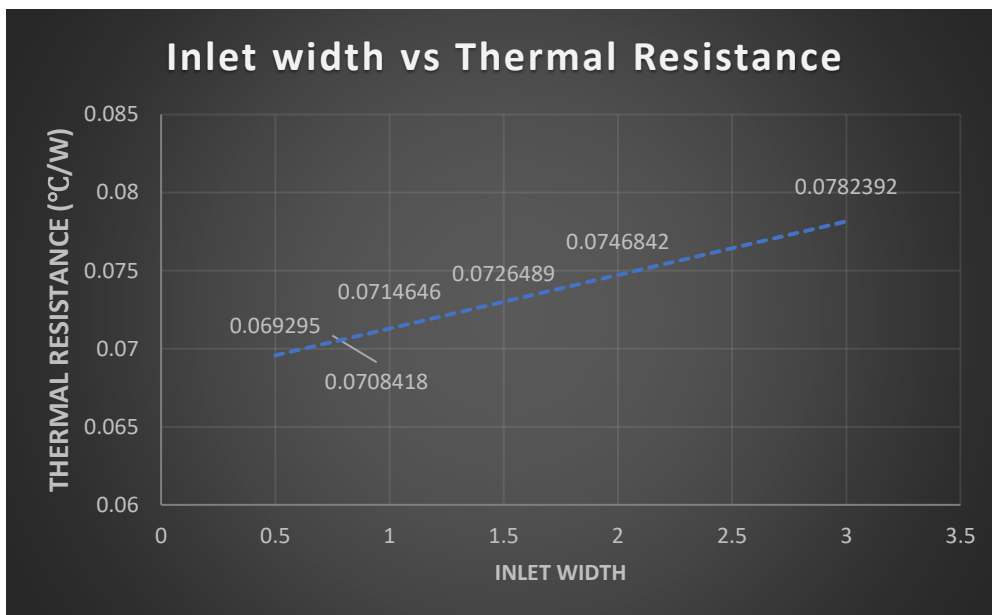


Figure 27 Variation in Maximum Temperature w.r.t. change in inlet width

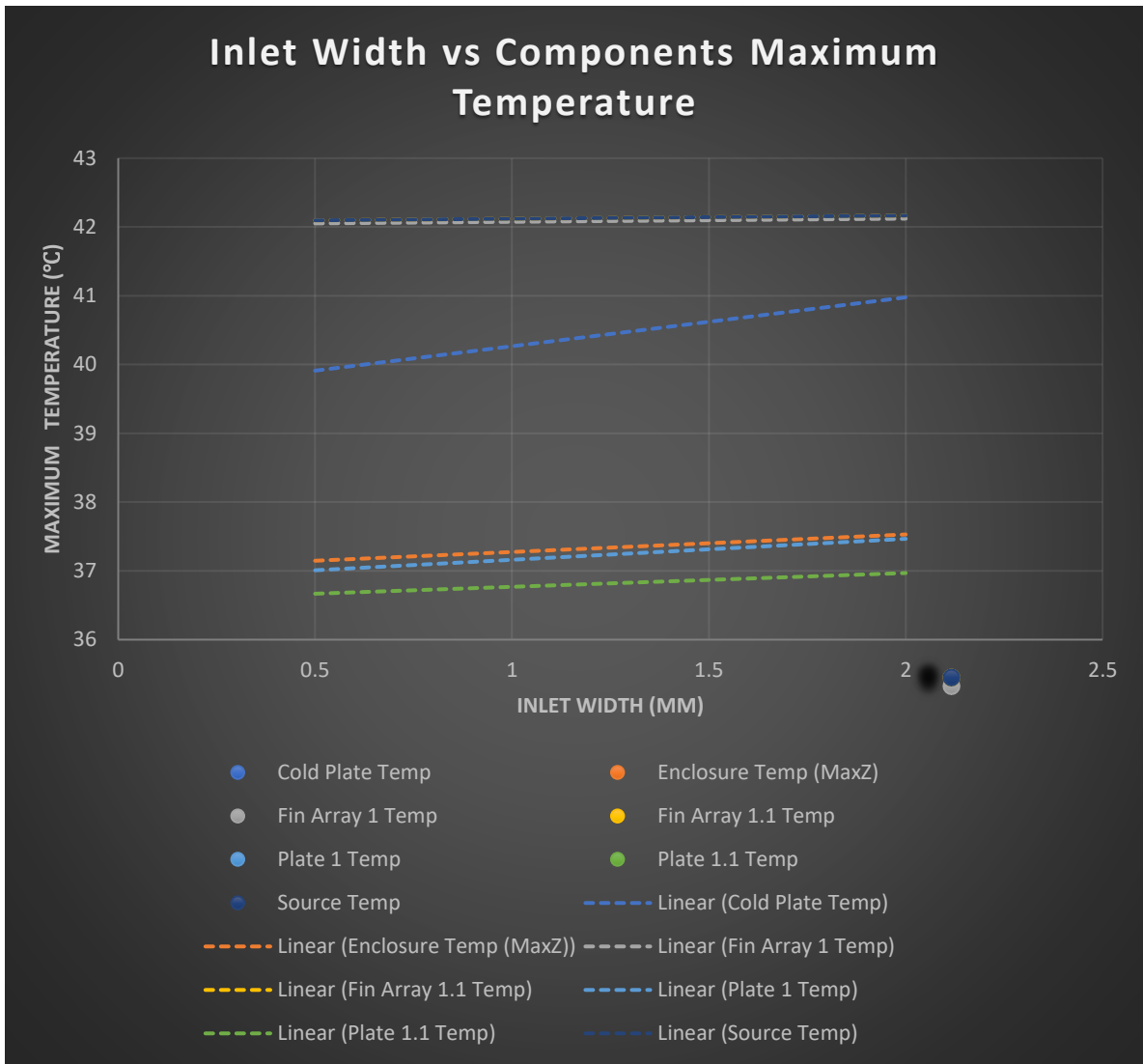




**Figure 28** Variation in Maximum Pressure w.r.t. change in inlet width



**Figure 29** Variation in Thermal Resistance of fins w.r.t. change in inlet width



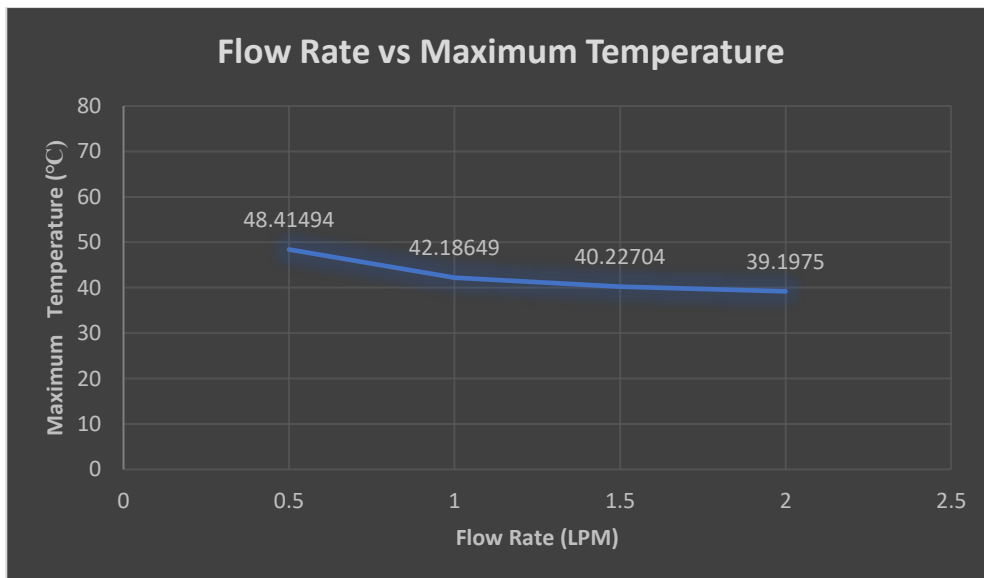
**Figure 30 Variation in Maximum Temperature of other components w.r.t. change in inlet width**

#### 4.4.2 Change in flow rate:

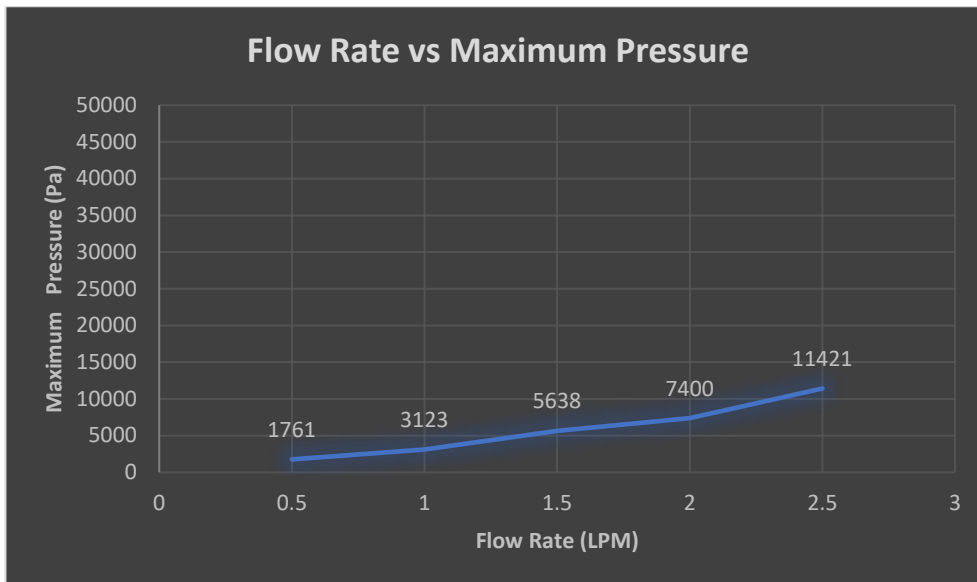
Here, the effect of varying the flow rate on maximum temperature, pressure and thermal resistance is observed keeping the geometry same as the original one. Hence, there is change in Reynolds number and Peclet number. Their values have been shown in table 5. The values indicate the flow still remains laminar for different flow rates. The following figures show how different flow rates have impact on these parameters.

**Table 5 Reynolds number and Peclet number for different flow rates**

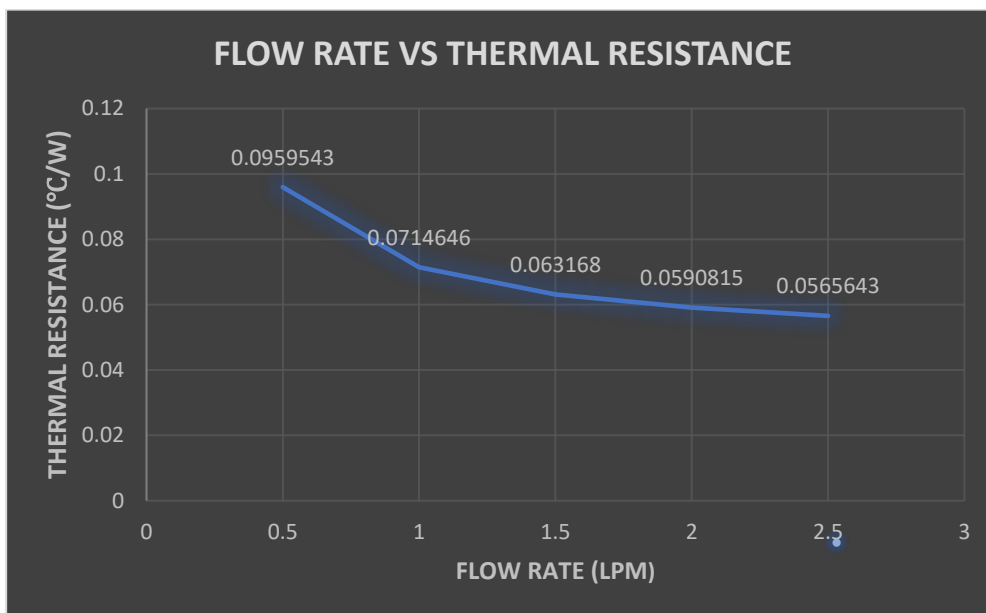
<b>Flow Rate (LPM)</b>	<b>Re</b>	<b>Pe</b>
0.5	230.71	2366.39
1	461.322	4731.77
1.5	692.131	7099.16
2	922.841	9465.55
2.5	1153.55	11831.9



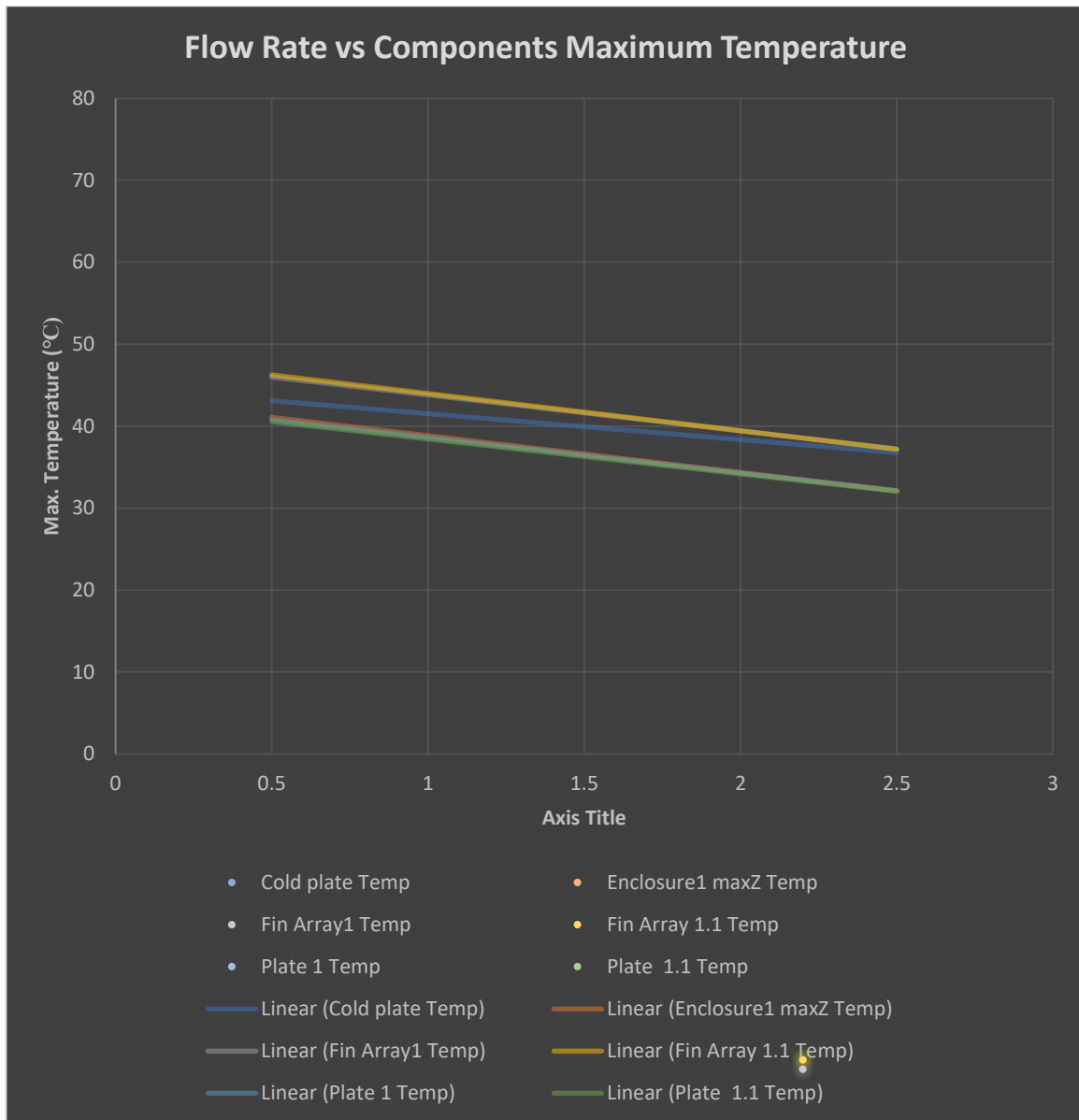
**Figure 31 Variation in Maximum Temperature w.r.t. change in flow rate**



**Figure 32 Variation in Maximum Pressure w.r.t. change in inlet width**



**Figure 33 Variation in Thermal Resistance of fins w.r.t. change in flow rate**



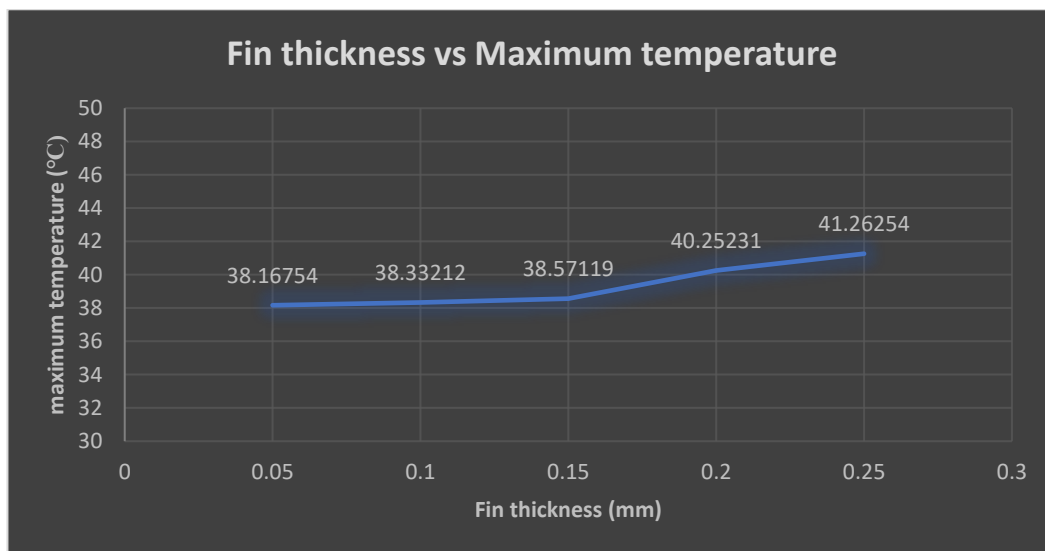
**Figure 34 Variation in Maximum Temperature of other components w.r.t. change in flow rate**

#### 4.4.3 Change in fin thickness:

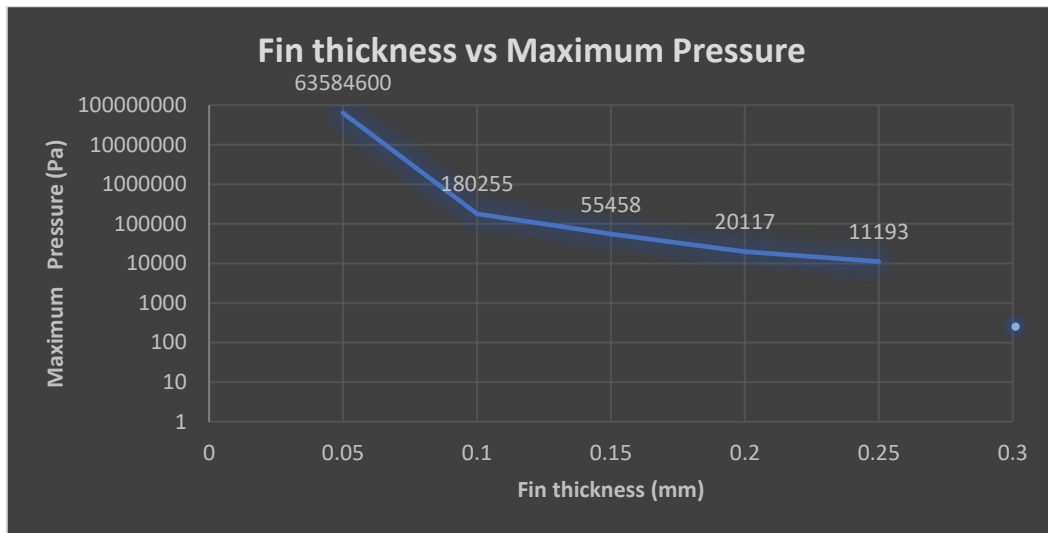
From previous case, we have taken the last reading as a setup for this. Here, the conditions are that the flow rate is constant at 2.5 LPM, the inlet width being 1mm as original and the fin thickness has been varied (aspect ratio is constant). Since, flow rate is constant, the Reynolds number and Peclet number will be constant from the previous case and will be 1153.55 and 11831.9 respectively. The fin thickness and number of fins relation is shown in table 6.

**Table 6 Fin thickness and number of fins per array**

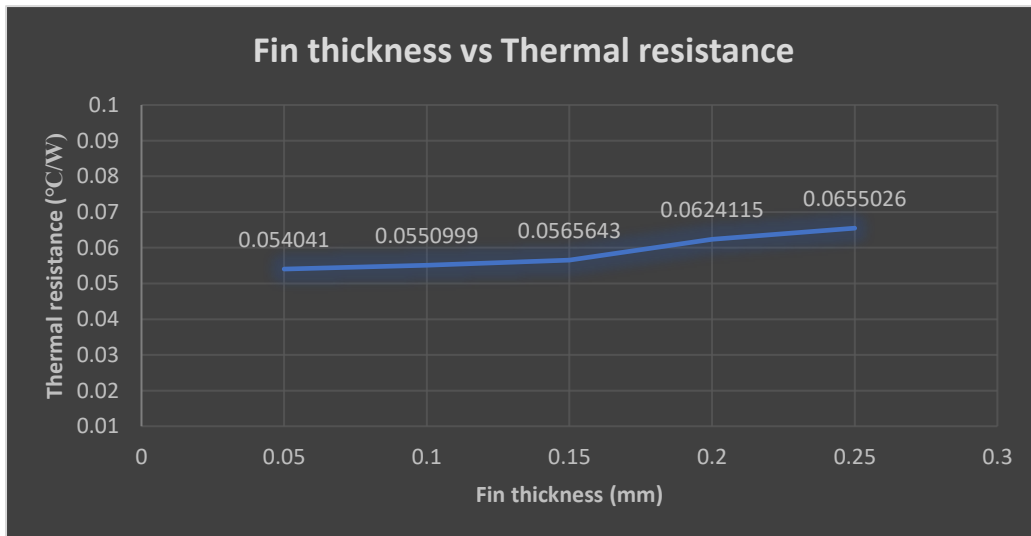
<b>Fin thickness/spacing</b>	<b>Number of fins per array</b>
0.05 mm	254
0.1 mm	127
0.15 mm	85
0.2 mm	64
0.25 mm	51



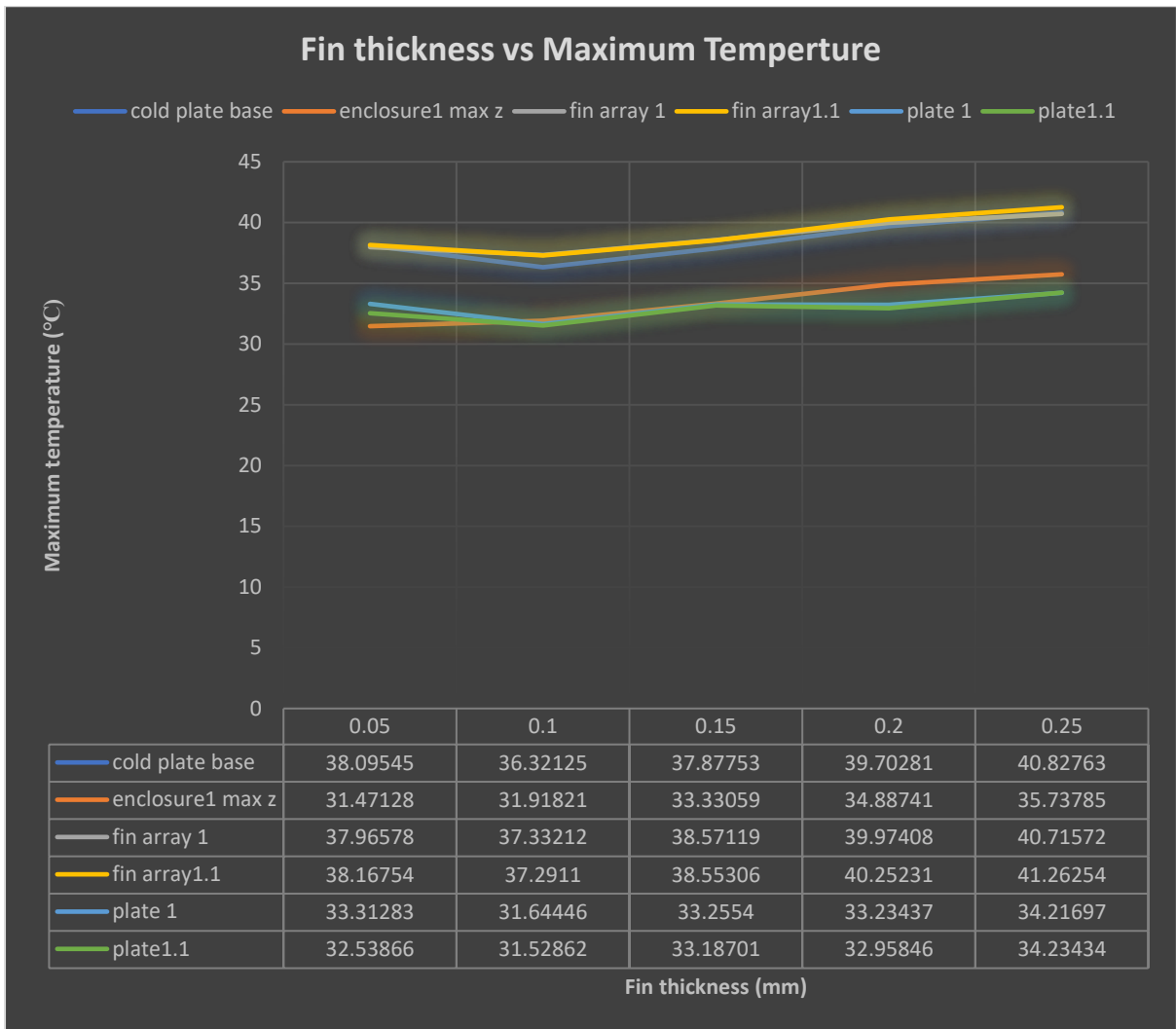
**Figure 35 Variation in Maximum Temperature w.r.t. change in fin thickness**



**Figure 36 Variation in Maximum Pressure w.r.t. change in fin thickness**



**Figure 37 Variation in Thermal Resistance of fins w.r.t. change in fin thickness**



**Figure 38** Variation in Maximum Temperature of other components w.r.t. change in fin thickness



## **CHAPTER 5**

### **POST-PROCESSING OF RESULTS**

The following observations have been made while optimizing the microchannel dimensions through analytical and numerical approach.

- 1) In the analytical approach, the total pressure drop comes around 930 Pa in which fins are accountable for 562 Pa of pressure drop while inlet area accounts for pressure drop of 368 Pa which is approximately 60% and 40% respectively. The same in numerical approach is differs by 5 to 6%.
- 2) While doing mesh sensitivity analysis, as the mesh size decreases the values of different parameters calculated in the solution changes but by a very small percentage.
- 3) While changing the inlet width of the flow area, it is observed that as the inlet width increases the maximum pressure decreases significantly while the maximum temperature and thermal resistance increase slightly.
- 4) In the case of varying the flow rate, the Reynolds number and Peclet number change every time. Further, as the flow rate increases, the maximum pressure increases drastically, while the thermal resistance and maximum temperature decrease slowly.
- 5) When the fin thickness is varied, the maximum pressure increases exponentially while the maximum temperature and the thermal resistance decrease drastically. Here, constant flow rate was considered.

## **CHAPTER 6**

### **CONCLUSION**

- An analysis was presented for evaluating the performance of microchannels in direct chip cooling application by considering the developing and fully developed laminar flow effects. The analysis included frictional pressure drop and the entrance and exit contraction and expansion losses.
- The results of numerical approach were presented as parametric plots to identify the desired channel width, fin thickness, and mass flow rate for a given heat load and channel depth using water as the cooling fluid.
- While considering both the approaches side by side, the analytical approach seems to be faster in computing the total pressure drop although it cannot pinpoint the maximum pressure point.
- The numerical approach is better for getting best visualization of results and can identify the points where the parameters reach their maximum and minimum values.
- Optimization of the setup done here by varying flow rate, inlet width and fin thickness can be continued further by changing aspect ratio in terms of height, fin gap or base thickness. Also, it can be done for a different cooling liquid instead of water which limits to single-phase cooling.
- Mesh sensitivity analysis can always prove to be useful for getting accuracy in the results.

## REFERENCES

- [1] Satish G. Kandlikar and Harshal R. Upadhye, "Extending the Heat Flux Limit with Enhanced Microchannels in Direct Single Phase Cooling of Computer Chips", 21st IEEE SEMI-THERM Symposium
- [2] Upadhye, H. R. and Kandlikar, S. G, "Optimization of Microchannel Geometry for Direct Chip Cooling Using Single Phase Heat Transfer," Proceedings of the Second International Conference on Microchannels and Minichannels, June 17-19, 2004, Rochester, NY USA ASME Publications, pp 679-68, 2004.
- [3] Kandlikar, S. G., and Grande, W. J., "Evaluation of Single Phase Flow in Microchannels for High Flux Chip Cooling – Thermohydraulic Performance Evaluation and Fabrication Technology," Heat Transfer Engineering, Vol. 25, No. 8, pp. 5-16, 2004.
- [4] Steinke, M. E. and Kandlikar, S. G, "Single-Phase Heat Transfer Enhancement Techniques in Microchannel and Minichannel Flows," Proceedings of the Second International Conference on Microchannels and Minichannels, June 17-19, 2004, Rochester, NY USA ASME Publications, pp 141-148, 2004.
- [5] A. Muhammad, D. Selvakumar and J. Wu, Numerical investigation of laminar flow and heat transfer in a liquid metal cooled mini-channel heat sink, International Journal of Heat and Mass Transfer, <https://doi.org/10.1016/j.ijheatmasstransfer.2019.119265>
- [6] Satish G. Kandlikar, "Design Considerations for Cooling High Heat Flux IC Chips With Microchannels", 10.1109/MDAT.2014.2299535, 13 January 2014
- [7] Jessica Gullbrand (Intel), Nigel Gore & Jason Matteson (Iceotope), Elizabeth Langer (CPC - Colder Products Company), "ACS Liquid Cooling Cold Plate Requirements", October 9, 2019

[8] Laxmidhar Biswal, Suman Chakraborty, and S. K. Som, “Design and Optimization of Single-Phase Liquid Cooled Microchannel Heat Sink”, 10.1109/TCAPT.2009.2025598

[9] Satish G. Kandlikar, Srinivas Garimella, Dongqing Li, Stéphane Colin and Michael R. King, “Heat Transfer and Fluid Flow in Minichannels and Microchannels”